LIMNOLOGY and OCEANOGRAPHY

ASLO

Limnol. Oceanogr. 9999, 2022, 1–16

doi: 10.1002/lno.12284

Elemental content allometries and silicon uptake rates of planktonic Rhizaria: Insights into their ecology and role in biogeochemical cycles

Manon Laget [1*] **Natalia Llopis-Monferrer** [2] **Jean-François Maguer** [2] **Aude Leynaert** [2] **Tristan Biard** [1]

[1]LOG, Laboratoire d'Océanologie et de Géosciences, Université du Littoral Côte d'Opale, Université de Lille, CNRS, IRD, UMR 8187, Wimereux, France

[2]Université de Brest, CNRS, IRD, Ifremer, LEMAR, Plouzané, France

Abstract

The last two decades have shown the importance of Rhizaria in the biogeochemical cycles of carbon and silicon in modern oceans. This eukaryotic supergroup, which includes Radiolaria and Phaeodaria, represents an important part of zooplanktonic carbon biomass and contributes to carbon and silica export. Still, accurate estimations of their carbon biomass are hindered by poor knowledge of their elemental composition, contrasting with well-established allometric carbon-to-volume relationships for smaller protists such as phytoplankton. Here, we directly measured carbon, nitrogen, and biogenic silica content as well as silicon uptake rates of planktonic Rhizaria. We highlight that size can be used as a predictor of elemental content for a broad variety of planktonic Rhizaria ranging from 200 μm to several mm, whereas size is weakly correlated with silicon uptake rates. Our results indicate that the scaling exponent of the carbon-to-volume allometry is significantly lower than those for smaller protists, underlining the low carbon strategy of these organisms. Still, we show that carbon and nitrogen densities span over four orders of magnitude, possibly accounting for the differences in depth ranges, nutritional modes and colonial or solitary forms. We estimate Rhizaria sinking speeds by combining carbon, nitrogen, and silica content data and show that great variability exists among the different taxa. Besides giving a better understanding of rhizarian ecology and biogeochemistry, these analyses, at the individual scale, are a first step to subsequent biomass and flux estimations at larger scales.

Marine plankton are a major reservoir of organic carbon (C) and nitrogen (N) and the main driver of the biological carbon pump, one of the mechanisms by which atmospheric CO_2 is transported to the deep ocean (Ducklow et al. 2001). In addition, many planktonic taxa require silicic acid to precipitate into biogenic silica (biogenic Si) to form skeletons, a process that has likely been responsible for a decline in silicic acid concentration in the oceans through geologic times (Siever et al. 1991). Therefore, knowledge of small-scale planktonic physiological processes is crucial for understanding the functioning of global oceanic biogeochemistry. Besides giving insights into organisms' physiology, quantifying the elemental composition and uptake rates of planktonic individuals is a key step to subsequently estimate stocks and fluxes at the population level. Allometric relationships scale traits of organisms with morphological criteria such as size over many orders of magnitude and are used for almost all forms of life (Brown et al. 2002). Accordingly, they enable elemental composition-to-volume relationships to provide trends that can be utilized in models. Indeed, size is a common trait in plankton community models (Finkel et al. 2009; Andersen et al. 2015) as well as in size-based ecosystem models (Blanchard et al. 2017), stressing the strength of this approach to provide model parameters. Allometric relationships linking individual C and N contents to cell volume relationships have been developed for diatoms and various protists; however, they are likely to overestimate elemental content of large protists such as Rhizaria (Menden-Deuer and Lessard 2000).

Planktonic representatives of Rhizaria are unicellular protists, with cell sizes ranging from a few tens of micrometers to several millimeters (Biard 2022*a*). Among them, Retaria includes Foraminifera and Radiolaria (Sierra et al. 2013).

*Correspondence: manon.laget@univ-littoral.fr

Additional Supporting Information may be found in the online version of this article.

Author Contribution Statement: T.B. and M.L. designed the study. M.L. and N.L.M. performed the sampling and filtrations. N.L.M. took the photographs and performed the incubations. J.F.M. was responsible for carbon and nitrogen content analysis. A.L. and N.L.M. were responsible for silica content and uptake rate analysis. M.L. performed image analysis, processed the data and wrote the manuscript. All authors edited the manuscript.

Foraminifera build calcium carbonate skeletons, whereas among Radiolaria, the skeleton is made of strontium sulfate for the order Acantharia and biogenic Si for the orders Nassellaria, Spumellaria, Collodaria, and Orodaria (Nakamura and Suzuki 2015; Suzuki and Not 2015; Biard 2022*b*). Phaeodaria, whose skeletons are made of biogenic Si, have long been considered radiolarians, but are now classified as Cercozoa, a sister group to Retaria (Sierra et al. 2013). Most rhizarians live as solitary cells, but some (e.g., collodarian families Collosphaeridae and Sphaerozoidae and the phaeodarian families Tuscaroridae and Medusettidae) are able to form large colonies (Nakamura and Suzuki 2015; Suzuki and Not 2015).

Despite their close morphologies, Phaeodaria and siliceous Radiolaria differ in their skeletal structure (Nakamura et al. 2018). Phaeodaria have porous skeletons that easily dissolve in seawater, whereas Radiolaria possess thick, dense skeletons that can preserve well in sediments and are commonly used in paleoclimate studies (De Wever et al. 2002). Even though diatoms account for the largest part of the biomass and production of biogenic Si (Tréguer et al. 2021), siliceous Rhizaria (i.e., siliceous Radiolaria and Phaeodaria) are the most silicified pelagic organisms known to date, considering the amount of silica per unit volume (Biard et al. 2018; Llopis-Monferrer et al. 2020). Partially because of these high biogenic Si densities, their skeleton is expected to act as ballast upon their death. Ultimately, skeletal remains increase fluxes of organic C and biogenic Si to the deep ocean, which will be integrated in seafloor sediments if not dissolved or remineralized on the way.

Siliceous Rhizaria inhabit the open ocean worldwide from the surface to the bathypelagic realm (Nakamura and Suzuki 2015; Suzuki and Not 2015; Biard 2022*b*). Their distribution is taxon dependent and influenced mostly by temperature, dissolved Si concentration and the amount of food available (Boltovskoy and Correa 2016; Biard and Ohman 2020). Although they all are heterotrophic, epipelagic radiolarian populations include many mixotrophic species, harboring a large diversity of algal symbionts (Decelle et al. 2015). On the other hand, deep-living populations are strictly heterotrophic, some also feed on sinking marine snow (Gowing 1986). For example, the phaeodarian family Aulosphaeridae can intercept on average 10% of total sinking flux at the depth of their maximum abundance, therefore reducing the efficiency of the biological carbon pump (Stukel et al. 2018). Despite their widespread occurrence in pelagic ecosystems, sampling and culturing them are challenging, hampering our knowledge of their biology and ecology. Still, over the last decade, non-destructive in situ imaging methods and environmental metagenomics have expanded understanding of their role at the community level. At a global scale, they represent a large part of mesozooplankton biomass (Biard et al. 2016) and could account for 2% to 19% of world biogenic Si production in the epipelagic layer (Llopis-Monferrer et al. 2020). Yet, substantial production by Rhizaria occurs below 200 m depth, where diatoms are absent. Furthermore, Rhizaria communities can contribute to a large component of vertical C export (Lampitt et al. 2009; Guidi et al. 2016; Gutierrez-Rodriguez et al. 2018). Large Phaeodaria (>1 mm) are responsible for up to 10% of the total organic C flux in the North Pacific by contributing to the enlargement and aggregation of sinking particles in the mesopelagic zone (Ikenoue et al. 2019).

Nevertheless, gaps remain in our knowledge of their organic C and N composition. Previous global C biomass assessments for large Rhizaria (Biard et al. 2016) relied upon a C-to-volume conversion factor of 80 μg C mm^{-3} measured on a variety of zooplanktonic organisms (Beers and Stewart 1970). In contrast, Stukel et al. (2018) demonstrated that flux feeders Aulosphaeridae (Phaeodaria) could meet their C demand only if their C density was one order of magnitude lower (1.1 μg C mm^{-3}, corresponding to 4.8 μg C cell^{-1} for a 2-mm cell). This revised estimate was further supported by an average C content of 13 μg C cell^{-1} measured on >1 mm Phaeodaria found in sediment traps (Ikenoue et al. 2019). In comparison, the equation provided by Menden-Deuer and Lessard (2000) gives a value of 234 μg C cell^{-1} for a 2-mm cell. Such high variability in conversion factors and its impact on biomass assessment emphasizes the need for accurate quantification of elemental content. To date, only three studies have provided C and N data from direct measurements, as well as estimates of C : N ratios (Michaels et al. 1995; Llopis-Monferrer et al. 2020; Mansour et al. 2021), but they focused solely on a few limited taxa. A robust tool that could be used in biogeochemical or size-based models is still lacking.

On the other hand, cell biogenic Si content correlates with cell volume over the entire size spectrum, including many taxa (Biard et al. 2018; Llopis-Monferrer et al. 2020; Llopis Monferrer et al. 2021). The silica-to-carbon ratio (Si : C) is lower than for diatoms, without significant regional variation, but it has only been investigated for the smallest taxa (Llopis Monferrer et al. 2021). Also, little is known about silicon uptake rates of siliceous Rhizaria (i.e., the rates at which they take up silicic acid to build their biogenic Si skeleton). In addition to knowing their silica biomass, such values are essential to understanding how they use silica from their environment at the physiological scale, opening the door to subsequent estimates of their turnover times, as well as to refining their role in the Si cycle. Likely because they are highly silicified cells, their Si uptake rate displays greater values than that of diatoms (Llopis Monferrer et al. 2021). Current data are too scarce to investigate a potential link with cell size or dissolved silica (dissolved Si) concentration in the ocean.

Here, using original and literature data, we investigate how size relates to elemental content for a broad variety of solitary and colonial Rhizaria. We also further examine the Si : C ratio and Si uptake rates. Finally, we discuss biogeochemical and ecological implications of these results.

Material and methods

Sampling

We collected 2036 Rhizaria specimens either in the coastal or oligotrophic waters of the California Current

Ecosystem (CCE) during the P2107 process cruise (July–August 2021, as part of the CCE-LTER program) onboard R/V *Roger Revelle* (Fig. 1a). We used various net tows to gather individuals from different depth intervals from the surface to as deep as 800 m (Supporting Information Table S1). In addition, we collected 55 individuals from the family Aulacanthidae (Phaeodaria) in the bay of Villefranche-sur-Mer (Mediterranean Sea, France; 43.69°N, 7.31°E; Fig. 1b) in 2019. Immediately after sampling, we isolated Rhizaria specimens under a stereomicroscope and rinsed them with filtered surface seawater. We then sorted individuals at the order, family or genus level based on the classifications from Nakamura et al. (2015) for Phaeodaria and from Suzuki and Not (2015) for Radiolaria (Fig. 2). Large Nassellaria (Radiolaria) found in the California Current were identified as *Phlebarachnium* sp. according to Strelkov and Reshetnyak (1959).

Organic C and N content

To obtain sufficient organic C and N matter for analysis, we deposited from 1 to 40 cells onto 25 mm GF/F filters that had been precombusted at 450°C for 4 h. Filters were placed in glass vials, previously washed for 24 h with HCl, rinsed with MilliQ water and combusted at 450°C for 4 h. The vials containing the dry filters were stored at −20°C and dried at 55°C overnight before analysis. Blank filters were prepared in the same way (i.e., combusted the same day and stored in the same conditions). C and N contents were quantified with a mass spectrometer (Delta plus, Thermo Fisher Scientific) coupled with a C/N analyzer (Flash EA, Thermo Fisher Scientific) via a Type III interface. Data were normalized to cell counts to obtain mean individual values (Q_C in μg C cell^{-1} or Q_N μg N cell^{-1}).

Biogenic Si content

The biogenic Si content of isolated Rhizaria was quantified according to Llopis-Monferrer et al. (2020). Briefly, we added 0.2 mL of 2.5 N hydrofluoric acid (HF) to the polymethylpentene tubes containing the filters with isolated specimens. The biogenic Si contained in the filters was then digested for 48 h at room temperature with HF acid to allow digestion of the robust Rhizaria skeletons. We then added 9.8 mL of saturated boric acid (H_3BO_3) solution to eliminate interference from HF in the subsequent colorimetric analysis for Si. Analyses were performed on a Technicon Auto-Analyzer II by colorimetric quantification of the orthosilicic acid (Aminot and Kérouel 2007). The standards used for calibration were prepared with the same matrix as for the samples (HF/H_3BO_3). As C and N data, biogenic Si concentrations were normalized to cell counts to obtain individual biogenic Si content (Q_{bSi} in μg bSi cell^{-1}).

Si uptake rates (ρ_{Si})

For these measurements, we used the radioisotope of Si (^{32}Si) following protocols previously described (Tréguer et al. 1991; Leynaert et al. 1996; Llopis-Monferrer et al. 2020). Briefly, samples containing from 1 to 30 individuals were spiked with a ^{32}Si silicic acid solution and incubated on deck for 24 h in a flowing-seawater incubator to maintain constant water temperature. After incubation, isotope samples were filtered by gentle (<150 mmHg) vacuum filtration onto 47 mm diameter, 0.6 μm pore-size polycarbonate membrane filters (Nuclepore), rinsed twice with filtered seawater to wash away nonparticulate ^{32}Si and dried at room temperature for 48 h. The activity of ^{32}Si in the samples was determined using the Cerenkov counting method (Leynaert 1993) on a scintillation counter (Tri-Carb 4910TR, Perkin Elmer) 3 months after the samples were filtered. Counts yielding less than three times

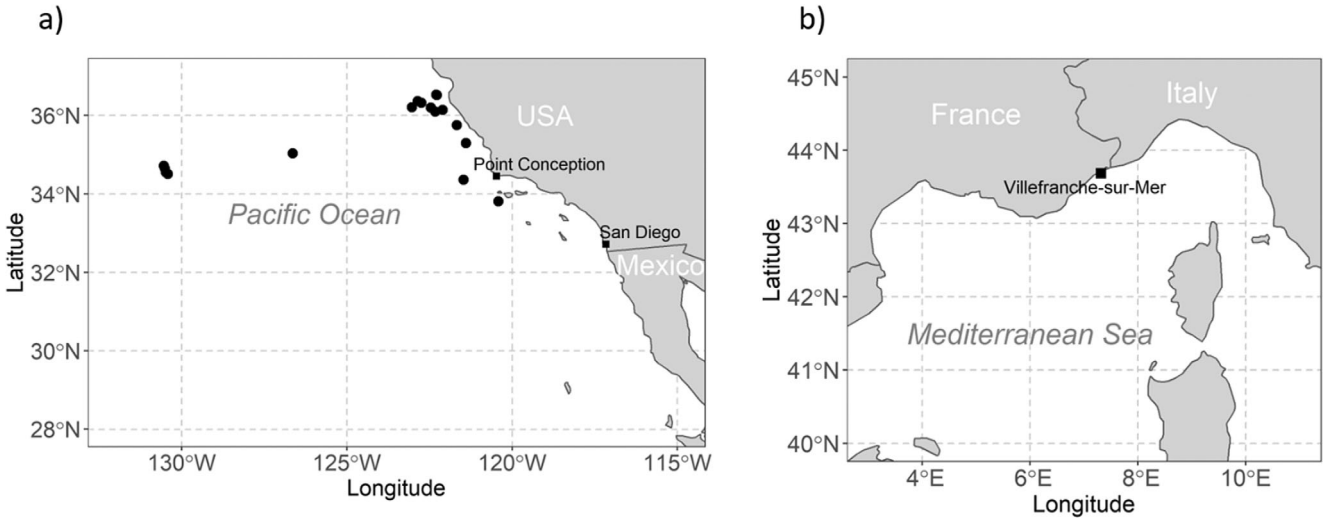

Fig. 1. Sampling locations for this study. (**a**) Sampling stations during the P2107 process cruise and, (**b**) location of Villefranche-sur-Mer, France.

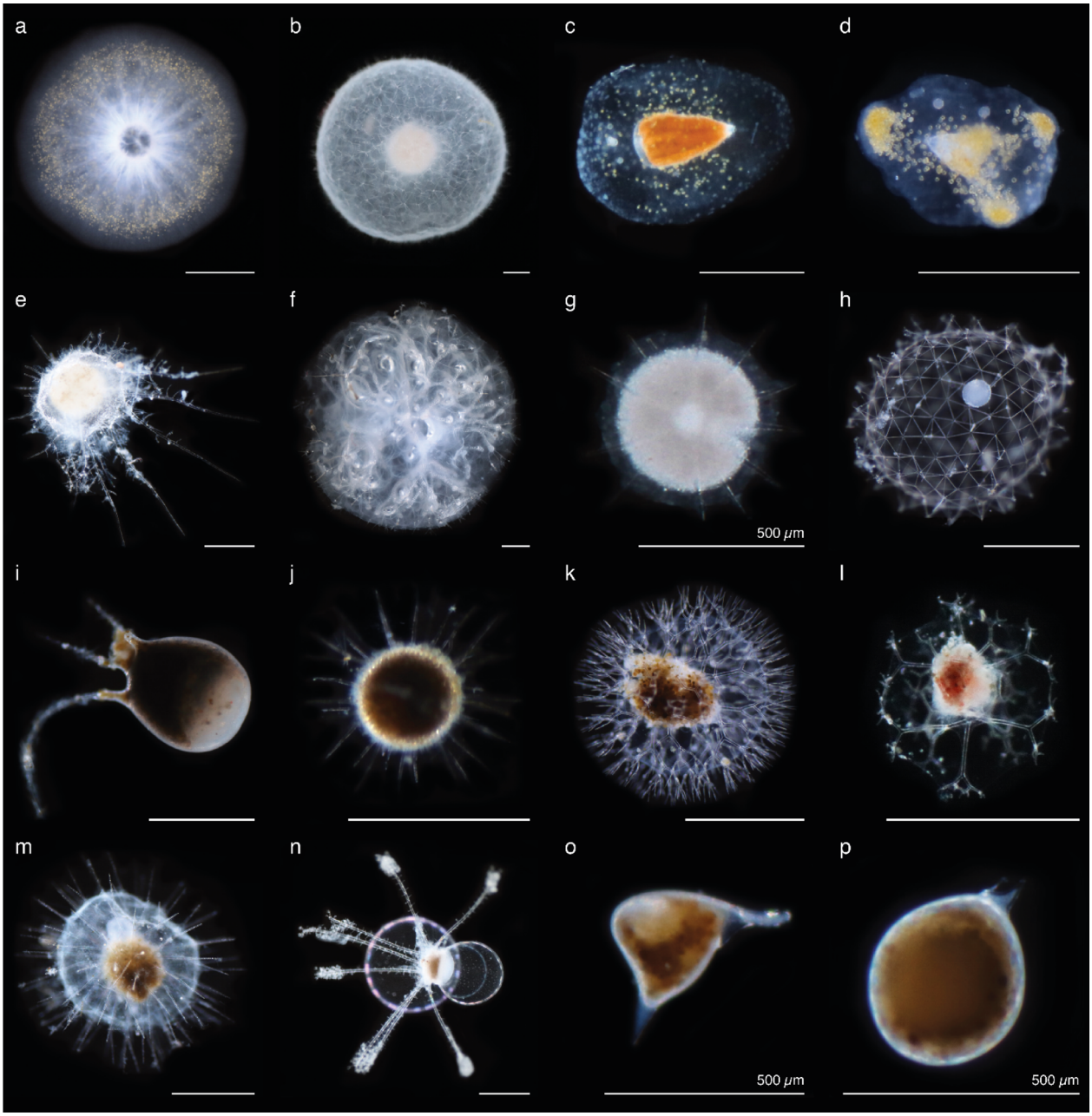

Fig. 2. Representatives of the sampled Rhizaria, observed under a stereomicroscope. (**a**–**g**) Radiolaria, (**h**–**p**) Phaeodaria. (**a**) *Thalassicolla* sp. (Collodaria), (**b**) *Thalassosphaera* sp. (Collodaria), (**c**,**d**) *Phlebarachnium* sp. (Nassellaria), (**e**) *Oroscena* sp. (Orodaria), (**f**) *Cytocladus* sp. (Orodaria), (**g**) Spumellaria, (**h**) Aulosphaeridae, (**i**) Tuscaroridae, (**j**) Castanellidae, (**k**–**l**) Coelodendridae, (**m**) Aulacanthidae, (**n**) Medusettidae, (**o**–**p**) *Protocystis* sp. (Challengeridae). All scale bars are 1 mm, unless otherwise indicated.

the background (23 CPM) were discarded. Results were normalized to cell counts to obtain individual uptake rates (ρ_{Si} in nmol Si cell^{-1} d^{-1}). Samples were then analyzed for biogenic Si content as previously described. The specific uptake rate (V_{Si} in d^{-1}) was calculated by normalizing the Si uptake rate to the biogenic Si concentration. Subsequently, we deduced the turnover time t as $(\ln 2/V_P)$ (in d).

Volume estimations

During the isolation process, photographs of each specimen were taken (Canon Eos 77D camera) to relate elemental data to various morphological criteria. From the pictures, we measured the length of major and minor axes using ImageJ software (Abràmoff et al. 2004). Volumes (V) were estimated by approximating the shape and size of each taxon using

simple geometric shapes that allowed calculation of the associated volume (Mansour et al. 2021; Supporting Information Fig. S1; Table S2). Finally, the equivalent spherical diameter (ESD) was determined from the volume (Supporting Information Eq. S1). All images used for measurements are available at https://doi.org/10.17882/89409.

Statistical analyses

We combined C and N content data measured for this study with literature data (Mansour et al. 2021). All data analyses were conducted using R software (R Core Team 2020).

To test the relationship between individual elemental content and volume, we assumed that it was adequately described by a power law:

$$Q_i = a \times V^b, \quad (1)$$

where Q_i is the individual C or N content in μg C cell^{-1} or μg N cell^{-1}, V is the individual volume in mm^3, a is the normalization constant, and b is the scaling exponent of the power law. We used $\log_{10}$-transformed elemental content and volume data, as this is the most appropriate method to assess allometric-scaling relationships (Kerkhoff and Enquist 2009). This led to the transformed equation:

$$\log_{10} Q_i = \log_{10} a + b \log_{10} V. \quad (2)$$

For these linear regression analyses, we choose Model I (ordinary least squares regression) instead of Model II, as Model I is largely recommended for application in allometry (Kilmer and Rodríguez 2017) and because measurement error of the independent variable, the individual volume, is considered to be low. Moreover, our purpose was to provide a predictive relationship. The linear models were validated by leave-one-out cross-validation using the R package *caret* (Kuhn et al. 2020) and by analysis of normality and homoscedasticity of residuals. We compared the regression slope of the C-to-volume relationship with those found previously for diatoms and various protists (Menden-Deuer and Lessard 2000) with Student's *t* tests. Difference in the regression slopes between Radiolaria and Phaeodaria was tested using ANOVA. We then calculated the C and N density in μg C mm^{-3} and μg N mm^{-3}, respectively, and tested for differences in mean values between taxa with ANOVA. We evaluated the correlation between Q_C and Q_N using a Kendall's τ correlation test.

To determine the Si : C ratio (mol : mol), we compiled our Q_{bSi} data with literature data (Biard et al. 2018; Llopis-Monferrer et al. 2020; Supporting Information Table S3) and when available, we calculated the ratio using the median values of C (in nmol C cell^{-1}) and biogenic Si content (in nmol Si cell^{-1}) for each taxon and geographic area. Excess densities were computed from C, N, and biogenic Si content according to Baines et al. (2010) and Stukel et al. (2018) (*see* details in Supporting Information Text S1). We then estimated the theoretical sinking U_{th} speed from Stokes' law.

Correlations between Si uptake rates ρ_{Si} and specific uptake rates V_{Si}, on the one hand, and cell volume and averaged daily silicic acid concentrations, on the other hand, were tested with a Kendall's τ correlation test. Dissolved Si concentrations were measured on water samples collected with Niskin bottles.

All the data and code used for these statistical analyses are available on GitHub (https://github.com/MnnLgt/Elemental_composition_Rhizaria).

Results

C and N contents and molar C : N ratio

We measured Q_C for 153 samples of pooled Rhizaria, corresponding to 1555 specimens from 8 families of Phaeodaria and 536 specimens belonging to the radiolarian orders Collodaria (Fig. 2a,b), Nassellaria (Fig. 2c,d), Orodaria (Fig. 2e,f), and Spumellaria (Fig. 2g). Q_N was quantified for 136 of the samples, corresponding to 2002 specimens covering the same taxonomic groups (Table 1). Overall, ESD covered almost three orders of magnitude (Table 1), ranging from 220 ± 60 μm for Spumellaria to 9.7 mm for *Cytocladus* sp. (Fig. 2f). We found the highest average Q_C and Q_N per taxon for solitary Collodaria (65.1 ± 32.8 μg C cell^{-1} and 15.4 ± 10.4 μg N cell^{-1}). The largest values, 717 μg C cell^{-1} and 76.8 μg N cell^{-1}, were measured for the only specimen of *Cytocladus* sp. (order Orodaria), which was large (diameter = 9.7 mm). The lowest Q_C and Q_N were observed for the phaeodarian genus *Protocystis* sp. (0.71 ± 0.37 μg C cell^{-1} and 0.12 ± 0.08 μg N cell^{-1}) (Table 1). The average C : N ratio was 7.8 ± 2.1, reaching its highest value for the nassellarian *Phlebarachnium* sp. (11.3 ± 2.8) and its lowest for solitary collodarians (5.7 ± 1.4) (Table 1).

Along with 103 samples available from the literature (Mansour et al. 2021; Table 1), we tested for the relationship between elemental composition and cell size using ordinary least-square regressions of $\log_{10}$-transformed C or N content on $\log_{10}$-transformed cell volume for a total of 256 samples for C and 235 for N. For both elements, we found a significant relationship ($R^2 = 0.76$, p-value < 0.0001, RMSE = 0.40 for C; $R^2 = 0.78$, p-value < 0.0001, RMSE = 0.41 for N), described by the equations:

$$\log_{10} Q_C = [0.455 \pm 0.016] \times \log_{10} V + [0.958 \pm 0.025], \quad (3)$$

$$\log_{10} Q_N = [0.477 \pm 0.017] \times \log_{10} V + [0.157 \pm 0.026], \quad (4)$$

where V is the volume in mm^3, Q_C is the individual C content in μg C cell^{-1}, and Q_N is the individual N content in μg N cell^{-1}. In both cases, residuals were normally distributed and showed homoscedasticity (Supporting Information Figs. S2, S3). These equations can be transformed into:

Table 1. Summary of carbon and nitrogen content (denoted Q_C and Q_N, respectively) data used for this analysis, compiled from Mansour et al. (2021) and this study. Elemental content and density are expressed as mean ± standard error.

				Carbon			Nitrogen				
Group	Order	Taxon	ESD (μm)	n_C*	Q_C (μg C cell^{-1})	Density (μg C mm^{-3})	n_N*	Q_N (μg N cell^{-1})	Density (μg N mm^{-3})	C : N (mol : mol)	Reference
Phaeodaria	Aulacanthida	Aulacanthidae	909 ± 671	34 [596]	5.8 ± 10.0	11.2 ± 8.8	23 [540]	1.2 ± 2.0	1.4 ± 0.6	7.0 ± 0.6	This study
		Aulacanthidae	733 ± 124	17 [302]	3.1 ± 1.6	18.0 ± 15.3	17 [302]	0.3 ± 0.2	1.8 ± 1.6	12.4 ± 2.3	Mansour et al. (2021)
	Phaeocalpida	Castanellidae	632 ± 89	35 [567]	7.4 ± 2.6	52.9 ± 13.1	34 [566]	1.1 ± 0.4	8.0 ± 2.1	7.7 ± 0.7	This study
		Tuscaroridae	1210 ± 93	7 [10]	45.3 ± 23.1	48.9 ± 25.1	7 [10]	7.5 ± 4.0	8.0 ± 3.9	7.1 ± 0.5	This study
	Phaeodendrida	Coelodendridae	1609 ± 695	13 [45]	12.5 ± 10.1	4.9 ± 2.1	9 [26]	2.6 ± 1.3	0.8 ± 0.3	7.8 ± 0.8	This study
		Challengeria sp.	184 ± 73	2 [48]	1.2 ± 1.4	241.2 ± 108.8	2 [48]	0.1 ± 0.1	14.6 ± 1.7	19.0 ± 6.6	Mansour et al. (2021)
		Medusettidae	1893 ± 456	3 [4]	23.8 ± 12.5	7.4 ± 4.1	3 [4]	4.1 ± 1.8	1.3 ± 0.7	6.7 ± 0.6	This study
		Protocystis sp.	318 ± 53	11 [213]	0.7 ± 0.4	39.7 ± 13.0	10 [200]	0.1 ± 0.1	6.1 ± 2.7	7.9 ± 2.0	This study
		Protocystis sp.	97 ± 8	12 [414]	0.7 ± 0.5	2224.4 ± 1283.2	12 [414]	0.1 ± 0.0	259.3 ± 131.4	10.0 ± 2.1	Mansour et al. (2021)
	Phaeosphaerida	Aulosphaeridae	1959 ± 206	10 [120]	2.3 ± 0.7	0.6 ± 0.2	10 [120]	0.4 ± 0.1	0.1 ± 0.0	6.5 ± 0.8	This study
Radiolaria	Acantharia	Various		18 [540]	0.2 ± 0.2						Mansour et al. (2021)
	Collodaria	Collosphaeridae (colonial)	94 ± 29	8 [15,033]	80.7 ± 41.2	0.6 ± 0.4	6 [14,589]	17.0 ± 4.5	0.1 ± 0.1	7.4 ± 2.0	Mansour et al. (2021)
		Solitary spp.	286 ± 404	2 [32]	21.6 ± 0.0	155.1 ± 47.7	2 [32]	3.7 ± 0.0	26.8 ± 8.2	6.8 ± 0.0	Mansour et al. (2021)
		Solitary spp.	3425 ± 558	13 [33]	65.1 ± 32.8	3.1 ± 1.9	13 [33]	15.4 ± 10.4	0.7 ± 0.5	5.7 ± 1.4	This study
		Sphaerozoidae (colonial)	116 ± 25	54 [41,111]	99.8 ± 87.5	1.9 ± 1.7	52 [39,511]	13.7 ± 8.2	0.4 ± 0.4	7.6 ± 3.1	Mansour et al. (2021)
	Nassellaria	Various	83 ± 6	6 [241]	0.5 ± 0.2	1472.1 ± 729.7	6 [241]	0.1 ± 0.0	171.3 ± 85.3	10.3 ± 1.7	Mansour et al. (2021)
		Phlebarachnium sp.	1175 ± 289	19 [468]	6.4 ± 1.6	8.9 ± 5.1	19 [468]	0.7 ± 0.3	0.9 ± 0.3	11.3 ± 2.8	This study
	Orodaria	*Cytocladus* sp.	9719	1 [1]	717.6	1.5	1 [1]	76.8	0.2	10.9	This study
		Oroscena sp.	1492 ± 571	5 [8]	44.3 ± 34.0	25.0 ± 14.1	5 [8]	7.2 ± 5.3	4.1 ± 2.4	7.2 ± 0.8	This study
	Spumellaria	Various	157 ± 38	2 [74]	0.8 ± 0.3	328.1 ± 126.9	2 [74]	0.1 ± 0.0	45.6 ± 32.5	9.7 ± 3.7	Mansour et al. (2021)
		Various	220 ± 60	2 [26]	1.5 ± 0.6	279.7 ± 104.8	2 [26]	0.3 ± 0.1	45.1 ± 14.4	7.2 ± 0.4	This study

*Number of samples analyzed, along with the total number of cells (in brackets).

$$Q_C = 10^{[0.958\pm0.025]} \times V^{[0.455\pm0.016]}, \quad (5)$$

$$Q_N = 10^{[0.157\pm0.026]} \times V^{[0.477\pm0.017]}. \quad (6)$$

Volume explained 76% and 78% of the total variance of Q_C and Q_N. For both relationships, the phaeodarian families Castanellidae and Tuscaroridae and the radiolarian order Orodaria were almost always found above the regression lines, whereas the phaeodarian family Aulosphaeridae was systematically below (Fig. 3).

Considering the whole dataset, the regression slopes of the individual element content-to-volume relationship were 0.455 and 0.477 for C and N, respectively (Eqs. 3, 4), but there was a significant difference in the slopes between Radiolaria and Phaeodaria (ANOVA: p-value = 0.006 for C, p-value < 0.0001 for N), with the highest slopes for Radiolaria (Supporting Information Table S4). This difference could be due in part to a potential effect of the uneven distribution of data from both groups along the size axis (Supporting Information Figs. S4, S5).

We compared the regression slope of the C-to-volume relationship (0.455; Eq. 3) with those obtained by Menden-Deuer and Lessard (2000). Ours differed significantly from the slopes obtained for diatoms (slope = 0.811; t-test: p-value < 0.0001) and other various protists (slope = 0.939; t-test: p-value < 0.0001).

C and N densities ranged over four orders of magnitude (Fig. 4) and mean values showed significant differences among taxa (ANOVA: p-value < 0.0001 for both C and N). The phaeodarian family Aulosphaeridae displayed the lowest average C density (0.56 ± 0.23 μg C mm^{-3}) and the collodarian family Collosphaeridae the lowest average N density (0.08 ± 0.06 μg N mm^{-3}). *Protocystis* sp. collected in the Southern Ocean and Nassellaria collected in the Mediterranean Sea reached the highest mean densities for both C and N (>1000 μg C mm^{-3} and >100 μg N mm^{-3}). In contrast, *Protocystis* sp. and the nassellarian *Phlebarachnium* sp. found in the CCE had much lower mean C (39.3 ± 12.5 and 8.9 ± 5.1 μg C mm^{-3}) and N (6.1 ± 2.7 and 0.9 ± 0.3 μg N mm^{-3}) densities (Table 1).

A Kendall's rank correlation τ test showed a strong significant correlation between Q_C and Q_N (τ = 0.91, p-value < 0.0001). Molar C : N ratios differed significantly among groups (ANOVA: p-value < 0.0001), even though they differed greatly within each group (Fig. 5; Supporting Information Fig. S6).

Biogenic Si content, molar Si : C ratios, and excess densities

We measured the Q_{bSi} for 68 samples, representing 802 individuals from 4 radiolarian taxa and 7 phaeodarian taxa. We

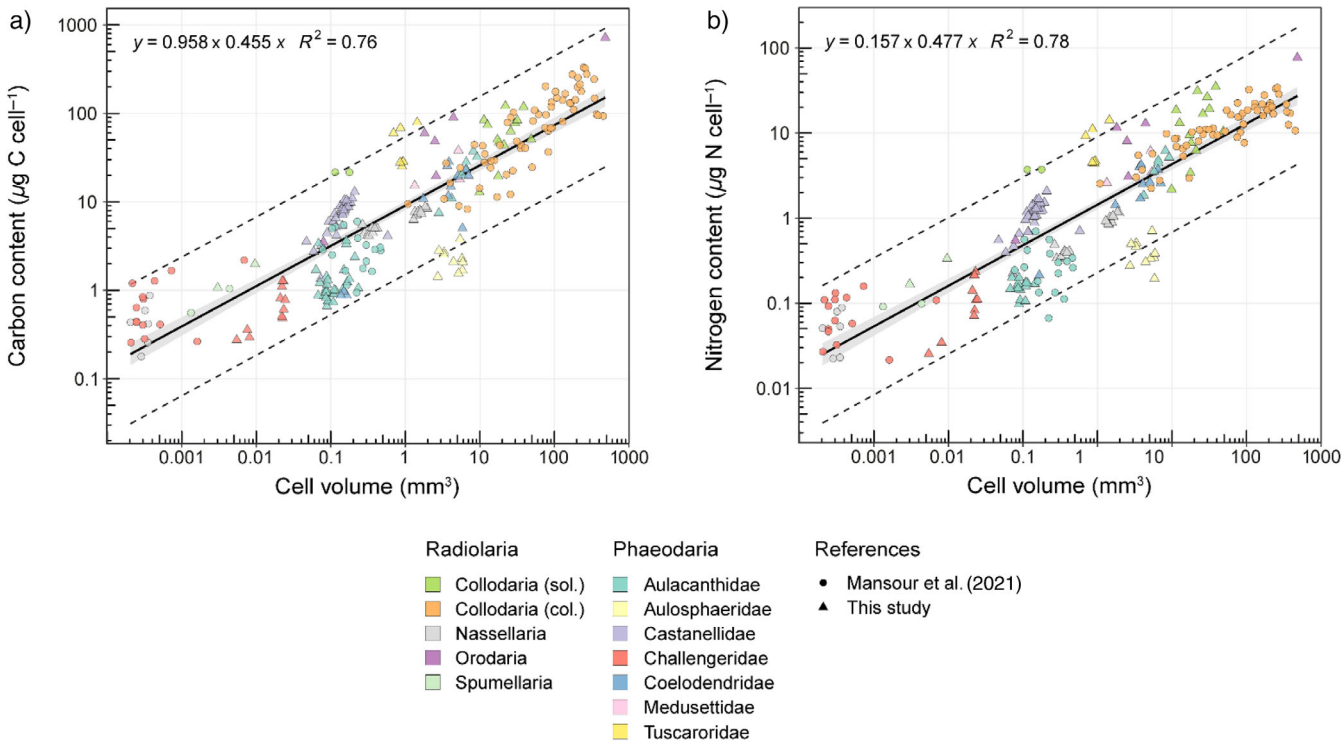

Fig. 3. General allometry for elemental composition of planktonic Rhizaria. (**a**) Carbon (μg C cell^{-1}) to volume (mm^3) and (**b**) nitrogen (μg N cell^{-1}) to volume (mm^3). Collodaria include solitary (sol.) and colonial (col.) specimens. Black solid lines represent the Model 1 least-squares regressions of $\log_{10}$-transformed data. Gray ribbons represent the 95% confidence level intervals and black dashed lines show the 95% prediction intervals. Data are compiled from Mansour et al. (2021) and this study.

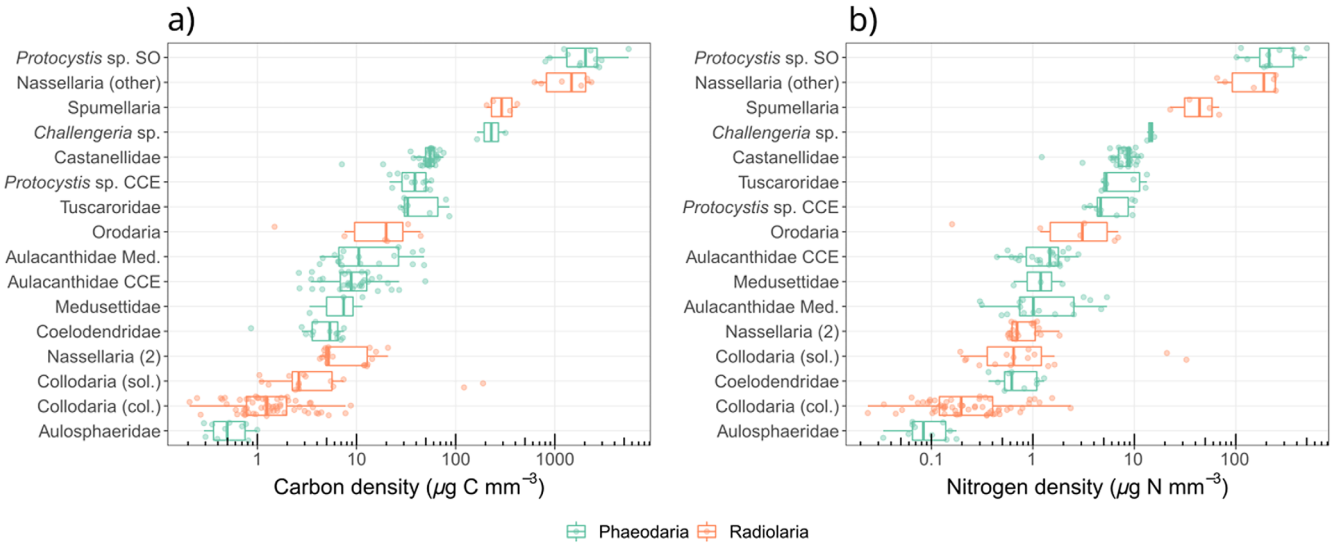

Fig. 4. Elemental densities for planktonic Rhizaria. (**a**) Carbon densities and (**b**) nitrogen densities. Nassellaria (2) refers to *Phlebarachnium* sp. Collodaria include solitary (sol.) and colonial (col.) specimens. The central value indicates the median. The lower and upper limits of the box correspond to the 25th and 75th percentiles. The lower whisker extends from the 25th percentile to the smallest value at most 1.5 × IQR (inter-quartile range) of the 25th percentile and the upper whisker extends from the 75th percentile to the largest value no further than 1.5 × IQR from the 75th percentile. Data are compiled from Mansour et al. (2021) and this study.

converted these data into μg Si cell^{-1} considering a molecular weight of 67 g mol^{-1} for hydrated amorphous silica (Mortlock and Froelich 1989) to include them in the regression equation linking Q_{bSi} (in μg Si cell^{-1}) to V (in μm^3) provided by Llopis-Monferrer et al. (2020). Our Q_{bSi} results ranged from 0.29 ± 0.16 μg Si cell^{-1} for *Phlebarachnium* sp. to 136 μg Si cell^{-1} for a solitary collodarian. By fitting a new model combining literature and new data, we observed that the new slope (0.55) did not show a significant difference from the previous one (0.52) (*t*-test: *p*-value = 0.83) (Supporting Information Fig. S7).

Using our data and literature data (Biard et al. 2018; Llopis-Monferrer et al. 2020), we could determine the molar Si : C ratio for seven phaeodarian families and the radiolarian orders

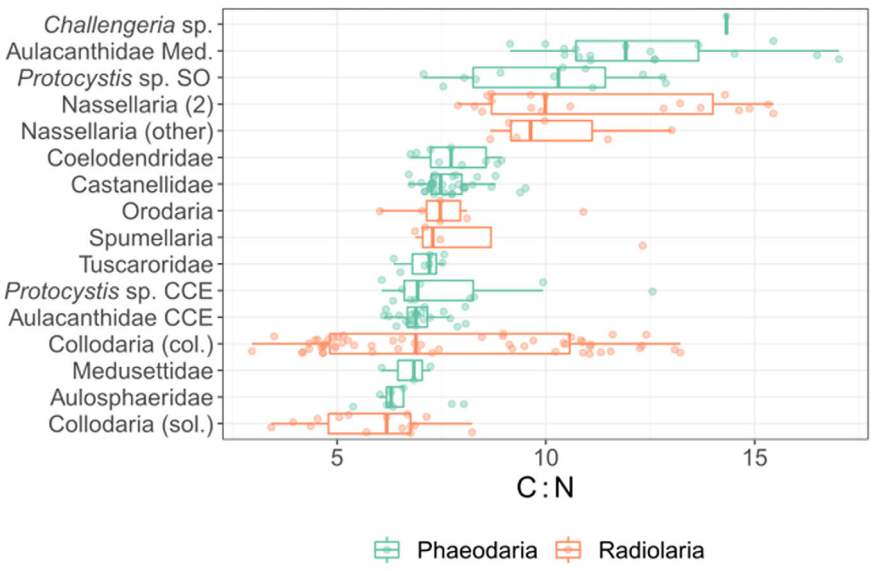

Fig. 5. C : N ratios (mol : mol) for planktonic Rhizaria. Nassellaria (2) refers to *Phlebarachnium* sp. Collodaria include solitary (sol.) and colonial (col.) specimens. The central value indicates the median. The lower and upper limits of the box correspond to the 25th and 75th percentiles. The lower whisker extends from the 25th percentile to the smallest value at most 1.5 × IQR (inter-quartile range) of the 25th percentile and the upper whisker extends from the 75th percentile to the largest value no further than 1.5 × IQR from the 75th percentile. Data are compiled from Mansour et al. (2021) and this study.

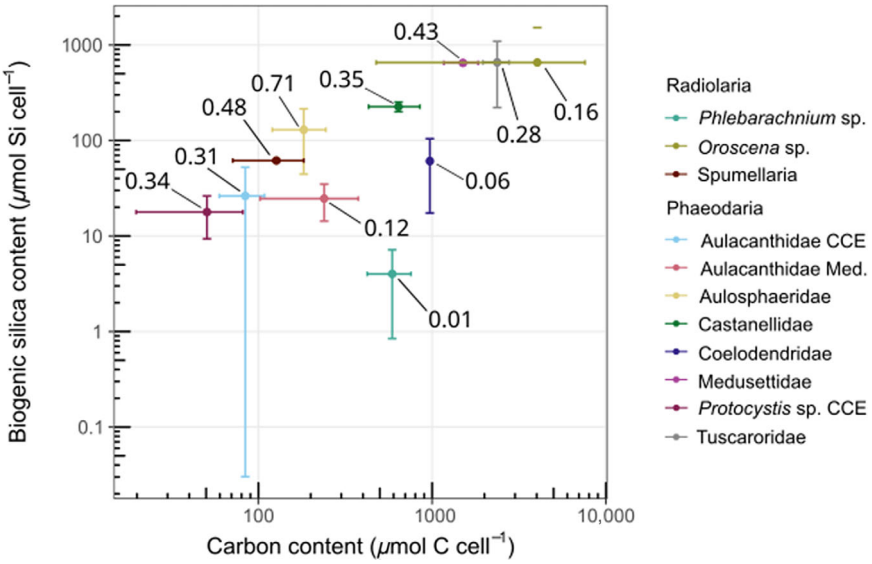

Fig. 6. General biogenic silica-to-carbon relationships for planktonic Rhizaria. Values are expressed as median biogenic silica (μmol Si cell^{-1}) and carbon (μmol C cell^{-1}) contents. Error bars show the median ± median absolute deviation of each distribution. Data are compiled from Biard et al. (2018), Llopis-Monferrer et al. (2020), Mansour et al. (2021), and this study.

Spumellaria and Orodaria (Fig. 6; Supporting Information Table S5). We did not consider Collodaria, as most specimens used for C analyses were not skeleton-bearing taxa. Aulosphaeridae reached the highest value (0.71) and the nassellarian *Phlebarachnium* sp. the lowest (0.01). Among phaeodarians, Coelodendridae displayed the lowest ratio (0.04) while Aulacanthidae showed a marked difference between specimens from the California Current (0.31) and the Mediterranean Sea (0.12).

Estimated excess densities ranged from 0.7 μg mm^{-3} for Coelodendridae to 545 μg mm^{-3} for Spumellaria (Table 2). Except for the latter and the phaeodarian Castanellidae, Tuscaroridae, and *Protocystis* sp., all excess densities were below 10 μg mm^{-3}. The lowest theoretical sinking speed was observed for the nassellarian *Phlebarachnium* sp. (20–43 m d^{-1}) and the highest for Tuscaroridae (883–2044 m d^{-1}).

Si uptake rates

We measured Si uptake rates ρ_{Si} for 26 samples corresponding to 347 cells belonging to 4 phaeodarian and 3 radiolarian taxa. Values ranged from 0.07 nmol Si cell^{-1} d^{-1} for our only sample of *Protocystis* sp. to 4.31 nmol Si cell^{-1} d^{-1}

Table 2. Excess densities and theoretical sinking speeds computed from Stokes' law for planktonic Rhizaria.

Group	Type	Area	ESD (μm)	Excess density (μg mm^{-3})	Theoretical sinking speed (m d^{-1})
Phaeodaria	Aulacanthidae	CCE	593	8.7 [4.0–42.7]	143 [66–707]
	Aulacanthidae	Med	679	5.6 [3.8–6.9]	121 [83–149]
	Aulosphaeridae	CCE	2076	1.0 [0.7–1.8]	199 [142–355]
	Castanellidae	CCE	648	57.0 [40.8–60.6]	1127 [806–1199]
	Coelodendridae	CCE	1930	0.7 [0.4–3.2]	115 [67–567]
	Medusettidae	CCE	2142	4.5 [4.5–4.6]	975 [973–986]
	Protocystis sp.	CCE	349	28.7 [25.5–54.2]	164 [146–311]
	Tuscaroridae	CCE	1177	27.8 [13.5–31.3]	1817 [883–2044]
Radiolaria	*Phlebarachnium* sp.	CCE	881	0.9 [0.6–1.2]	33 [20–43]
	Oroscena sp.	CCE	1682	9.8 [5.3–14.0]	1298 [709–1864]
	Spumellaria	CCE	197	545 [543–546]	1001 [999–1004]

Med, Mediterranean Sea.
Data used are compiled from Biard et al. (2018), Llopis-Monferrer et al. (2020), Mansour et al. (2021), and this study. ESD is the median ESD. Excess densities were calculated with the medians of carbon content, silica content and volume data. Between brackets are the excess densities calculated with the 1st and 3rd quantiles of carbon content and silica content, and associated sinking speeds.

Table 3. Silicic acid uptake rates ρ_{Si}, specific silicic acid uptake rates V_{Si}, and turnover times t for planktonic Rhizaria and diatoms.

Group	Type	Area	n	ρ_{Si}* (nmol Si cell^{-1} d^{-1})	V_{Si}* (d^{-1})	t (d)	Reference
Phaeodaria	Aulacanthidae	CCE	4	0.46 ± 0.70	0.008 ± 0.008	87	This study
	Aulacanthidae	Med			0.061 ± 0.089	11	Llopis-Monferrer et al. (2020)
	Aulosphaeridae	CCE	6	0.62 ± 0.54	0.006 ± 0.007	116	This study
	Castanellidae	CCE	3	0.17 ± 0.11	0.0007 ± 0.0005	990	This study
	Protocystis sp.	CCE	1	0.07	0.002	347	This study
	Protocystis sp.	Med			0.167 ± 0.148	4	Llopis-Monferrer et al. (2020)
Radiolaria	Collodaria	CCE	1	4.31	0.002	347	This study
	Collodaria	Med			0.422 ± 0.312	2	Llopis-Monferrer et al. (2020)
	Phlebarachnium sp.	CCE	10	0.31 ± 0.25	0.065 ± 0.035	11	This study
	Nassellaria	Med			0.086 ± 0.021	8	Llopis-Monferrer et al. (2020)
	Oroscena sp.	CCE	1	0.81	0.0007	990	This study
	Spumellaria	Med			0.372 ± 0.348	2	Llopis-Monferrer et al. (2020)
Diatoms		Various			0.06–1.80	0.4–11.6	*See* references in Llopis-Monferrer et al. (2020)

Med, Mediterranean Sea.
*ρ_{Si} and V_{Si} are denoted ρ_P and V_P in Llopis-Monferrer et al. (2020).
Except for diatoms, ρ_{Si} and V_{Si} are expressed as mean ± standard error. t is determined from mean V_{Si}. *See* Supporting Information Table S6 for details of biogenic silica content Si uptake rates.

for our only sample of *Thalassosphaera* sp. (solitary Collodaria) (Supporting Information Table S6). The specific uptake rate V_{Si} spanned three orders of magnitude, with a minimal value for Orodaria and Castanellidae (0.0007 d^{-1}) and a maximal value for the nassellarian *Phlebarachnium* sp. (0.06 ± 0.03 d^{-1}) (Table 3). This corresponds to a turnover time ranging from 10 to 1061 d (Table 3). Average daily silicic acid concentration (Supporting Information Table S7) showed no correlation with ρ_{Si} (Kendall's $\tau = -0.04$, p-value = 0.79) and a weak correlation with V_{Si} (Kendall's $\tau = -0.55$, p-value = 0.0001). When merged with 31 data points available from literature, cell volume showed a very weak positive correlation with ρ_{Si} ($\tau = 0.24$, p-value = 0.008) and a weak negative correlation with V_{Si} ($\tau = -0.50$, p-value < 0.0001).

Discussion

Elemental composition and stoichiometry of planktonic Rhizaria

In this study, we successfully measured C and N contents for 2091 rhizarian specimens covering 12 taxa. By combining these data with literature data, we found that over a size range extending three orders of magnitude (100 μm to 10 mm), the Q_C and Q_N values for Rhizaria can be reliably predicted from cell volume (Fig. 3). We report here a C : V scaling exponent for Rhizaria (0.455) which is significantly lower than those found for diatoms (0.811) and other protists (0.939) (Menden-Deuer and Lessard 2000), supporting the conclusion that the equations for diatoms are not suited for these giant protists. From our results, the scaling exponents for the two rhizarian lineages Radiolaria and Phaeodaria differ significantly, being higher for Radiolaria; however, since we could not rule out the possibility of a bias due to differences in samples sizes, we recommend the use of the general relationship. Individual volume did not fully explain the variations in elemental composition ($R^2 = 0.76$ and 0.78 for the $Q_C : V$ and $Q_N : V$ relationships), with the remaining unexplained variability potentially linked to taxa-specific differences or physiological state of specimens. However, our purpose here was to determine general trends to provide a basis for comparison, even if specific taxa may deviate from them.

These differences between taxa were also reflected in elemental densities, which varied over four orders of magnitude (Table 1). The lowest mean C density (0.56 ± 0.23 μg C mm^{-3}) observed for the phaeodarian family Aulosphaeridae is one order of magnitude lower than the conversion factor (80 μg C mm^{-3}) used for the global assessment of Rhizaria biomass (Biard et al. 2016). However, it corroborates the density value of 1.1 μg C mm^{-3} based on the assessment of their C demand (Stukel et al. 2018). For a 2-mm cell, our allometry gives a C content of 17.4 μg C cell^{-1} while our mean Q_C for Aulosphaeridae is 2.3 μg C cell^{-1}. The value of 4.8 μg C cell^{-1} calculated by Stukel et al. (2018) falls within this range. This low value can be explained by the ratio of the central mass diameter, which consists of the central capsule and the phaeodium and is likely to contain most of the organic matter of the cell, to the skeleton diameter. In comparison, the family Aulacanthidae, known to co-occur with Aulosphaeridae in the California Current (Biard and Ohman 2020) and for which the combination of the central capsule and phaeodium occupies about half of the skeleton, has a mean C density of 11.2 ± 8.8 μg C mm^{-3}, a value one to two orders of magnitude

higher than for Aulosphaeridae. The other phaeodarian families containing large species (i.e., Castanellidae and Tuscaroridae), for which organic matter almost entirely fills the skeleton, have a mean C density of 52.9 ± 13.1 and 48.9 ± 25.1 μg C mm^{-3}. For these taxa, our observations are consistent with values measured on a bulk > 1-mm Phaeodaria population dominated by the same taxa in the North Pacific Ocean, but for which the taxon-specific Q_C values are not known (7.2–25 μg C cell^{-1}; Ikenoue et al. 2019). In contrast, the smallest phaeodarian group of our study, *Protocystis* sp. collected in the Southern Ocean (mean ESD = 97 μm), reaches the highest C and N densities (>1000 μg C mm^{-3}, >100 μg N mm^{-3}), probably because the organic matter occupies the entire cell. Among Radiolaria, Nassellaria other than *Phlebarachnium* sp. are the most C and N dense (>1000 μg C mm^{-3}, >100 μg N mm^{-3}), which could also be explained by organic matter entirely filling the skeleton. Foraminifera, the sister clade of Radiolaria among Retaria that builds $CaCO_3$ skeletons, have a mean C density of 89 μg C mm^{-3} (Michaels et al. 1995) which is a higher value than those reported for colonial and solitary Collodaria as well as Orodaria and photosymbiotic Nassellaria, but one to two orders of magnitude lower than C densities of Spumellaria and other Nassellaria.

For all taxa, the high variability in intragroup elemental densities is also reflected in regional differences. For example, the observed difference between *Protocystis* sp. collected in the CCE and those collected in the Southern Ocean, of one order of magnitude for both C and N, suggests that polar species are denser than their relatives living in warmer waters. Intragroup variability was previously observed for solitary Collodaria (9–280 μg C mm^{-3}; Michaels et al. 1995) and is most likely explained by environmental or cellular conditions. Indeed, it has been shown that life history or nutritional status, such as the composition of the phaeodium that is used to store food in Phaeodaria (Gowing 1986), could influence the Q_C and Q_N values as well as the C : N ratios (Sterner and Elser 2017).

Our results showed that Q_C and Q_N values were strongly correlated, but their ratio did not seem to be linked with size. Mean C : N ratios (mol : mol) are within the range of values reported for Radiolaria (Michaels et al. 1995) and showed significant variations among taxa. Overall, the mean C : N ratio (7.8 ± 2.1) is higher than the Redfield ratio of 6.6 (Redfield 1934), as well as C : N ratios for smaller protists (3.4–6.5; Menden-Deuer and Lessard 2000) and the mean ratio for all zooplankton (4.9; Kiørboe 2013). Elemental stoichiometry of phytoplankton is known to depend on environmental conditions such as N availability (Finkel et al. 2009). We can hypothesize that such effects could impact nutrient assimilation and thus growth rates for Rhizaria as well, but knowledge about physiological processes of Rhizaria is lacking.

Our values of Q_{bSi} fit well with the established allometric relationship (Biard et al. 2018; Llopis-Monferrer et al. 2020), underlining the robustness of this tool. Except for the photosymbiotic nassellarian *Phlebarachnium* sp. and the phaeodarian families Coelodendridae and Aulacanthidae from the Mediterranean Sea, all molar Si : C ratios were higher than those reported for diatoms (0.13 ± 0.04; Brzezinski 1985). This result is expected since we showed that Rhizaria have overall a low Q_C value and they are known to be the most highly silicified pelagic organisms per unit volume (Llopis-Monferrer et al. 2020). The high variations in molar Si : C ratios among taxa highlight the morphological as well as ecological diversity of these organisms. These ratios are likely to also be influenced by abiotic factors (e.g., temperature or nutrient availability), as stated by Brzezinski (1985) for diatoms, or biotic factors such as exposure to predation (Pondaven et al. 2007). Our data are based on individuals coming from different depths and different environmental conditions; thus, we still need to better constrain such factors in order to account for intragroup variability.

From individual to global biomass and flux estimations

Accurate global biomass estimations are needed to better constrain ecological as well as biogeochemical roles of marine organisms. Today, in situ imaging allows quantification and distinction at low taxonomic level of large Rhizaria as well as measurement of their biovolume (Nakamura et al. 2017; Biard and Ohman 2020). Following our measurements of elemental composition on individual Rhizaria, it is very likely that previous global C biomass assessments based on in situ imaging (Biard et al. 2016; Drago et al. 2022) need to be revised. Indeed, all giant Phaeodaria (> 600 μm) sampled by this method have a C density much lower (ranging from 0.6 ± 0.2 μg C mm^{-3} for Aulosphaeridae to 52.9 ± 13.1 μg C mm^{-3} for Castanellidae; Table 1) than the conversion factor used previously (80 μg C mm^{-3}). Nevertheless, it is important to note that small Rhizaria (< 600 μm), currently not reliably sampled by in situ imaging, are mostly much more C-dense, but their regional and global biomass and contribution to fluxes remain poorly constrained. For example, Radiolaria Polycystinea (including Nassellaria, Spumellaria, and Collodaria) are abundant in the first 100 m of the global tropical and subtropical ocean (Boltovskoy 2017) and, to our knowledge, their biomass has never been accurately assessed.

When computing biomass over a large spatial scale, choosing whether to use taxon-specific conversion factors or allometric relationships is not trivial. Errors in biomass estimations at the individual scale will propagate and be responsible for under or over estimations at the global scale. Using allometry can introduce variability especially for taxa deviating from the regression line; however, identification to the genus, species, or family level is not always possible as it relies on skeletal details that are generally not visible with in situ imaging instruments. Allometry thus provides a way to infer the biomass of a related organism. Moreover, allometric relationships are a straightforward way to compute the bulk biomass of a population. In the future, the availability of taxon-specific conversion factors as well as allometric relationships for C, N,

and biogenic Si will allow us to refine regional or global mass estimations with greater accuracy.

From biomass estimations, the next step is to assess the magnitude of export to the deep ocean. In addition to their mass, fluxes of particles are mainly determined by their sinking speed and their abundance. Although the last parameter is not in the scope of this study, constraining the elemental composition of an organism allows an initial estimate of its excess density with respect to the surrounding water (Baines et al. 2010) and thus its theoretical sinking speed determined from Stokes' law. Our computed excess densities for the Aulosphaeridae, Coelodendridae, and *Phlebarachnium* sp. are consistent with a previous estimated value for Aulosphaeridae (0.72 μg mm^{-3}; Stukel et al. 2018). Still, the other taxa displayed an excess density 1–3 orders of magnitude higher (Table 2). This variability between taxa is reflected in their estimated theoretical sinking speeds, which span three orders of magnitude. These results are expected, as the silica skeleton, which is the main ballast of the cell, shows large structural variations among taxa. Phaeodaria have a porous skeleton, whereas Radiolaria have a dense skeleton (Nakamura et al. 2018). This could explain why Spumellaria (Radiolaria) have a theoretical sinking speed one order of magnitude higher than specimens of *Protocystis* sp. (Phaeodaria), of comparable size. It would take 5 d for one spumellarian cell to sink from the upper mesopelagic to more than 5000 m depth, whereas it would take about 16 d for *Protocystis* sp. The same order of magnitude difference is observed between the radiolarian *Oroscena* sp. and the phaeodarian families Coelodendridae and Aulosphaeridae. However, the phaeodarian families Castanellidae, Tuscaroridae and Medusettidae, known to be more silica-dense (Biard et al. 2018), have a theoretical sinking speed ranging from $\sim$ 800 to $\sim$ 2000 m d^{-1}. Together with the radiolarian Spumellaria and *Oroscena* sp., their very high sinking speeds, coupled with their high elemental content, indicate that these taxa could be efficient exporters of organic matter and biogenic Si to the deep ocean upon their death. Even though Phaeodaria show higher dissolution rates than Radiolaria (Erez et al. 1982), they would quickly transit to great depths where loss caused by dissolution is lower than in surface waters because of colder temperatures and higher nutrient concentrations. Furthermore, their heavy skeleton likely prevents the organic matter of the cell from being remineralized along the way. In contrast, the other phaeodarian taxa and the nassellarian *Phlebarachnium* sp. have a much lower theoretical sinking speed. Therefore, because of their fragile nature, the delicate skeletons of Aulosphaeridae, Aulacanthidae, and Coelodendridae probably entirely dissolve on descent and never reach the seafloor. We can thus hypothesize that not all Rhizaria contribute equally to vertical export. Further investigation combining abundance data and dissolution rates should bring to light the relative contribution of each. Overall, the sinking rates we have calculated for Spumellaria, Castanellidae, and *Protocystis* sp. are one order of magnitude higher than those measured experimentally by Takahashi and Honjo (1983). Nevertheless, the values that they calculated from Stokes' law conformed to ours. For most taxa, they noted that the ratios of measured sinking speeds to theoretical sinking speeds were below 1, with great variations among taxa. Therefore, it is likely that our data are maximal values. Indeed, Stokes' law assumes that particles are perfect spheres and the morphology of planktonic Rhizaria can deviate significantly from this shape. The presence of skeletal ornamentation such as spicules or spines increases the drag of the cell, slowing it down. Moreover, Stokes' law predicts that the sinking speed of a sphere is proportional to the square of its radius, but it has been shown for diatoms that this exponent in fact varies between 1 and 2 (Miklasz and Denny 2010).

Si uptake rates and turnover times

Si uptake rate ρ_{Si} was only weakly positively correlated with size and not with silicic acid concentration. Specific Si uptake rate V_{Si} showed a weak but significant negative correlation with size, a pattern consistent with observed allometric scaling of nutrient uptake for phytoplankton (Edwards et al. 2012). Still, the weakness of the correlation indicates that other parameters may influence uptake rates. The significant, but also weak, correlation with silicic acid concentrations suggests that environmental conditions influence V_{Si}. However, care should be taken as dissolved Si concentrations were daily averages over large depth ranges. Our measured specific uptake rates V_{Si} were low (0.0007–0.06 d^{-1}) compared to those measured on small Rhizaria (Llopis-Monferrer et al. 2020) and diatoms (summarized in Claquin et al. 2006). It seems paradoxical that these silica-rich organisms take up dissolved Si at such a slow rate. Nonetheless, many Rhizaria live below the epipelagic layer, where diatoms are absent and where competition for silicic acid is expected to be limited. This may explain why *Phlebarachnium* sp., which competes with diatoms in the surface layer, have the highest V_{Si}. To date, very little is known about Si uptake dynamics of rhizarians, nor about cell lifespan. Laboratory studies on a few radiolarian species have shown no evidence of enhanced skeletal growth with higher silicate concentrations (Sugiyama and Anderson 1997). It is possible that there are phases in the life cycle where the consumption of Si is more important than at other times. Our measurements are first estimates that will be refined once we succeed in cultivating these cells over a longer period of time, with cells that reproduce. Until now, we have only kept them alive for 1–2 weeks and reproduction has never been observed.

Rhizaria are known to have SIT-L Si transporters (Marron et al. 2016), but the number of uptake sites as well as their affinity with dissolved Si are unknown. There is evidence that uptake affinity in phytoplankton does not scale linearly with cell size (Lindemann et al. 2016). Thus, it is not because Rhizaria are larger that their affinity with dissolved Si is higher. In addition, the number of nutrient uptake sites and their specific affinity are expected to decrease with cell size

(Fiksen et al. 2013). If this is also true for Si, it could partially account for the negative correlation between cellular volume and specific uptake rate. This could also help explain why larger individuals take up Si at a slower rate comparatively to their size. Further investigation of uptake processes at the cellular level as well as uptake kinetics, either through modeling or experimental observations, should shed light on the observed values. Such refinements should ultimately enhance understanding of their consequences at a population scale.

From our data, estimated turnover times t extended between 10 and > 1000 d. These values are higher than for phytoplanktonic organisms, which usually range from a few hours to a few days (Flynn et al. 2018). This result is to be expected since these organisms are much larger and are thus expected to have a slower growth rate. Skeletal composition should follow the same pattern, so the organism can keep its equilibrium Si : C ratio. Many of our observed values are nevertheless much higher than expected. For a protist, a turnover time longer than 100 d seems unrealistic. Net sampling could have damaged some cells, although we took care during the sampling process. Moreover, some of the organisms were sampled in the mesopelagic layer, which could have altered their physiological state during recovery. However, collection depth ranges using net tows were too broad to investigate a potential effect of sampling depth (Supporting Information Table S8). Our results also question the way we calculated turnover rates, which assumes constant growth and binary fission. However, production of swarmers has been observed in both Phaeodaria and Radiolaria (Nakamura and Suzuki 2015; Yuasa and Takahashi 2016). In fact, V_{Si} might not be constant over time: swarmers or juvenile cells could silicify at high rates when producing the skeleton, but then silicification could be reduced at a minimal rate once the skeleton is formed. On the other hand, if the Si transporters in planktonic Rhizaria take up a constant amount of dissolved Si per unit of time, regardless of the life stage of the individual, this would then imply that V_{Si} decreases as the cell grows. Therefore, differences with literature data (Llopis-Monferrer et al. 2020) may be the result of differences in cell growth stage, as well as environmental differences. The evolution of V_{Si} with time has not yet been investigated. Doing so would require culturing Rhizaria, which has barely been successful so far, with a few in vivo experiments maintaining Radiolaria for up to 23 d (Anderson et al. 1989). Overall, these results highlight the strategy of low mass, low growth rate of these organisms. Further analysis of their Si and C uptake rates will provide insight into the life cycle of these organisms, as well as about their ecology.

Insights into the ecology of planktonic Rhizaria

By scaling elemental composition to individual size over several orders of magnitude, empirical allometric relationships provide clues to underlying processes that govern the ecology of planktonic Rhizaria. The scaling exponents of the C to V and N to V relationships are much lower than one, meaning that elemental content does not increase in proportion to cell volume. Moreover, the C-to-volume exponent is significantly lower than for smaller protists, implying a low C strategy for this planktonic group, as previously suggested (Menden-Deuer and Lessard 2000; Stukel et al. 2018). This difference could be explained by several factors. Rhizaria can be either heterotrophic or mixotrophic and many taxa feed on sinking marine snow or are diffusion feeders (Gowing 1986). Their large size, from 100 μm to several mm, is responsible for an increased gap between nutrient delivery, depending on the cross-section area of the organism (Jackson 1993), and food demand, related to its volume. However, since most of the organic matter is located within the central part of the cell, increasing the radius allows a wider intercepting cross-section and a higher potential clearance rate for these non-swimming organisms, whereas this enlarged body is compensated by a low C density. In addition, it has been suggested that cells with little organic matter are less attractive and more difficult for predators to grasp (Kiørboe 2013), in addition to their large size making them less accessible to small grazers. Only a few predators have been reported for Radiolaria (summarized in Biard 2022*b*) and even less for Phaeodaria, which are usually larger organisms than Radiolaria. As proposed by Stukel et al. (2018), another advantage of this low C strategy is the maintenance of neutral buoyancy. This would allow them to stay at their optimal depth range, which can be restricted for some Phaeodaria because of abiotic factors as well as the presence of food (Biard and Ohman 2020). Low C density could counteract the presence of a silica skeleton, which increases the overall density of the cell. This could be an explanation of the high molar Si : C ratios, in comparison with diatoms, that we observed for most taxa. Therefore, in addition to the presence of spicules and other skeletal elements, as well as the porous skeleton in Phaeodaria, a lower organic matter density diminishes the sinking speed, while the inflated volume increases the drag of the organism.

Even though the C-to-volume regression equation provides a general trend, it does not fully explain the variations among data, drawing attention to taxon-specific characteristics (Fig. 3). This result contrasts with the lower scatter of C content data along the regression line for diatoms and other protists (Menden-Deuer and Lessard 2000). These differences are not surprising, since the taxa considered in the present study encompass various depth ranges, from the surface to the mesopelagic (Biard and Ohman 2020), two nutrition modes (mixotrophy and strict heterotrophy) and colonial and solitary individuals. Thus, several taxa are systematically lower or higher than the regression line (e.g., Aulosphaeridae, Castanellidae), accounting for their taxon-specific particularities. Notably, several points belonging to the family Aulosphaeridae are outside the 95% prediction interval. These results are also reflected in the C and N densities spanning four orders of magnitude. Symbiont-bearing taxa (Collodaria, *Phlebarachnium* sp.) are among the least C and N dense. In particular, the

photosymbiotic nassellarian *Phlebarachnium* sp. showed C and N densities two orders of magnitude lower than other Nassellaria. One hypothesis is that these taxa need to maintain neutral buoyancy to stay in surface waters and allow their symbionts to photosynthesize, which could also be facilitated by the presence of the gelatinous matrix along the presence of large lipid vacuoles in Collodaria (Anderson 1983). Conversely, deep living populations must generally adapt to a food-depleted environment, as well as colder temperature, which could lead to lower metabolic rates. Therefore, we can hypothesize that not only size, but also morphology and trophic strategy have consequences for cell composition and stoichiometry, and that the relative effect of each variable needs to be further examined.

Conclusion

From direct measurements of C and N content and literature data, we provided allometric relationships linking C and N composition to size for a broad variety of Rhizaria ranging from 100 μm to several mm in size, completing the allometric relationship relating biogenic Si content to volume. These simple equations that focus on size rather than species identity are powerful tools to be implemented in models. The combination of the three allometries is of key interest to improve estimates of rhizarian biomass, which have been poorly constrained in the past because of the lack of reliable conversion factors. In contrast, we have measured Si uptake rates and found that they are weakly correlated with size, likely because of the influence of other physiological processes and environmental variables that need to be further explored. From elemental data, we estimated the sinking speed of Rhizaria and showed that they can be fast exporters of organic matter and biogenic Si to the bottom of the ocean. Overall, our study highlights the low-C and slow-growth strategy of these large protists. These results will improve future assessments of the biomass of planktonic Rhizaria as well as refinement of understanding of their physiology and ecology.

Data availability statement

Data and scripts used for analyses are available in the GitHub repository https://github.com/MnnLgt/Elemental_composition_Rhizaria. All images used for morphometric measurements were deposited in the SEANOE database at https://doi.org/10.17882/89409.

References

Abràmoff, M. D., P. J. Magalhães, and S. J. Ram. 2004. Image processing with ImageJ. Biophotonics Int **11**: 36–42.

Aminot, A., and R. Kérouel. 2007. Dosage automatique des nutriments dans les eaux marines: Méthodes en flux continu. Editions Quae.

Andersen, K. H., D. L. Aksnes, T. Berge, Ø. Fiksen, and A. Visser. 2015. Modelling emergent trophic strategies in plankton. J. Plankton Res. **37**: 862–868. doi:10.1093/plankt/fbv054

Anderson, O. 1983. Radiolaria. Springer.

Anderson, O. R., P. Bennett, and M. Bryan. 1989. Experimental and observational studies of radiolarian physiological ecology: 3. Effects of temperature, salinity and light intensity on the growth and survival of *Spongaster tetras tetras* maintained in laboratory culture. Mar. Micropaleontol. **14**: 275–282. doi:10.1016/0377-8398(89)90014-5

Baines, S. B., B. S. Twining, M. A. Brzezinski, D. M. Nelson, and N. S. Fisher. 2010. Causes and biogeochemical implications of regional differences in silicification of marine diatoms. Global Biogeochem. Cycl. **24**: GB4031. doi:10.1029/2010GB003856

Beers, J. R., and G. L. Stewart. 1970. The ecology of the plankton off La Jolla, California, in the period April through September 1967. Bull. Scripps Inst. Oceanogr. **17**: 67–87.

Biard, T. 2022*a*. Rhizaria, p. 1–11. *In* eLS. Wiley.

Biard, T. 2022*b*. Diversity and ecology of Radiolaria in modern oceans. Environ. Microbiol. **24**: 2179–2200. doi:10.1111/1462-2920.16004

Biard, T., and others. 2016. In situ imaging reveals the biomass of giant protists in the global ocean. Nature **532**: 504–507. doi:10.1038/nature17652

Biard, T., J. W. Krause, M. R. Stukel, and M. D. Ohman. 2018. The significance of giant phaeodarians (Rhizaria) to biogenic silica export in the California Current Ecosystem. Global Biogeochem. Cycl. **32**: 987–1004. doi:10.1029/2018gb005877

Biard, T., and M. D. Ohman. 2020. Vertical niche definition of test-bearing protists (Rhizaria) into the twilight zone revealed by in situ imaging. Limnol. Oceanogr. **65**: 2583–2602. doi:10.1002/lno.11472

Blanchard, J. L., R. F. Heneghan, J. D. Everett, R. Trebilco, and A. J. Richardson. 2017. From bacteria to whales: Using functional size spectra to model marine ecosystems. Trends Ecol. Evol. **32**: 174–186. doi:10.1016/j.tree.2016.12.003

Boltovskoy, D. 2017. Vertical distribution patterns of Radiolaria Polycystina (Protista) in the World Ocean: Living ranges, isothermal submersion and settling shells. J. Plankton Res. **39**: 330–349. doi:10.1093/plankt/fbx003

Boltovskoy, D., and N. Correa. 2016. Biogeography of Radiolaria Polycystina (Protista) in the world ocean. Prog. Oceanogr. **149**: 82–105. doi:10.1016/j.pocean.2016.09.006

Brown, J. H., V. K. Gupta, B.-L. Li, B. T. Milne, C. Restrepo, and G. B. West. 2002. The fractal nature of nature: Power laws, ecological complexity and biodiversity. Philos. Trans. R. Soc. Lond. B Biol. Sci. **357**: 619–626. doi:10.1098/rstb.2001.0993

Brzezinski, M. A. 1985. The Si:C:N ratio of marine diatoms: Interspecific variability and the effect of some environmental variables. J. Phycol. **21**: 347–357. doi:10.1111/j.0022-3646.1985.00347.x

Claquin, P., A. Leynaert, A. Sferratore, J. Garnier, and O. Ragueneau. 2006. Physiological ecology of diatoms along the river–sea continuum, p. 121–138. *In* The Silicon cycle: Human perturbations and impacts on Aquatic systems. Island Press.

De Wever, P., P. Dumitrica, J. P. Caulet, C. Nigrini, and M. Caridroit. 2002. Radiolarians in the sedimentary record. CRC Press.

Decelle, J., S. Colin, and R. A. Foster. 2015. Photosymbiosis in marine planktonic protists, p. 465–500. *In* Marine protists. Springer Japan. doi:10.1007/978-4-431-55130-0_19

Drago, L., and others. 2022. Global distribution of zooplankton biomass estimated by in-situ imaging and machine learning. Front. Mar, p. 871. doi:10.3389/fmars.2022.894372

Ducklow, H., D. Steinberg, and K. Buesseler. 2001. Upper ocean carbon export and the biological pump. Oceanography **14**: 50–58. doi:10.5670/oceanog.2001.06

Edwards, K. F., M. K. Thomas, C. A. Klausmeier, and E. Litchman. 2012. Allometric scaling and taxonomic variation in nutrient utilization traits and maximum growth rate of phytoplankton. Limnol. Oceanogr. **57**: 554–566. doi:10.4319/lo.2012.57.2.0554

Erez, J., K. Takahashi, and S. Honjo. 1982. In-situ dissolution experiment of radiolaria in the central North Pacific Ocean. Earth Planet. Sci. Lett. **59**: 245–254. doi:10.1016/0012-821x(82)90129-7

Fiksen, Ø., M. J. Follows, and D. L. Aksnes. 2013. Trait-based models of nutrient uptake in microbes extend the Michaelis-Menten framework. Limnol. Oceanogr. **58**: 193–202. doi:10.4319/lo.2013.58.1.0193

Finkel, Z. V., J. Beardall, K. J. Flynn, A. Quigg, T. A. V. Rees, and J. A. Raven. 2009. Phytoplankton in a changing world: Cell size and elemental stoichiometry. J. Plankton Res. **32**: 119–137. doi:10.1093/plankt/fbp098

Flynn, K. J., D. O. F. Skibinski, and C. Lindemann. 2018. Effects of growth rate, cell size, motion, and elemental stoichiometry on nutrient transport kinetics. PLoS Comput. Biol. **14**: e1006118. doi:10.1371/journal.pcbi.1006118

Gowing, M. M. 1986. Trophic biology of phaeodarian radiolarians and flux of living radiolarians in the upper 2000 m of the North Pacific central gyre. Deep Sea Res. Part A Oceanogr. Res. Pap. **33**: 655–674. doi:10.1016/0198-0149(86)90059-2

Guidi, L., and others. 2016. Plankton networks driving carbon export in the oligotrophic ocean. Nature **532**: 465–470. doi:10.1038/nature16942

Gutierrez-Rodriguez, A., M. R. Stukel, A. L. dos Santos, T. Biard, R. Scharek, D. Vaulot, M. R. Landry, and F. Not. 2018. High contribution of Rhizaria (Radiolaria) to vertical export in the California Current Ecosystem revealed by DNA metabarcoding. ISME J. **13**: 964–976. doi:10.1038/s41396-018-0322-7

Ikenoue, T., K. Kimoto, Y. Okazaki, M. Sato, M. C. Honda, K. Takahashi, N. Harada, and T. Fujiki. 2019. Phaeodaria: An important carrier of particulate organic carbon in the mesopelagic twilight zone of the North Pacific Ocean. Global Biogeochem. Cycles **33**: 1146–1160. doi:10.1029/2019gb006258

Jackson, G. A. 1993. Flux feeding as a mechanism for zooplankton grazing and its implications for vertical particulate flux. Limnol. Oceanogr. **38**: 1328–1331. doi:10.4319/lo.1993.38.6.1328

Kerkhoff, A. J., and B. J. Enquist. 2009. Multiplicative by nature: Why logarithmic transformation is necessary in allometry. J. Theor. Biol. **257**: 519–521. doi:10.1016/j.jtbi.2008.12.026

Kilmer, J. T., and R. L. Rodríguez. 2017. Ordinary least squares regression is indicated for studies of allometry. J. Evol. Biol. **30**: 4–12. doi:10.1111/jeb.12986

Kiørboe, T. 2013. Zooplankton body composition. Limnol. Oceanogr. **58**: 1843–1850. doi:10.4319/lo.2013.58.5.1843

Kuhn, M., and others. 2020. Package "caret". R J. **223**: 7.

Lampitt, R. S., I. Salter, and D. Johns. 2009. Radiolaria: Major exporters of organic carbon to the deep ocean. Global Biogeochem. Cycl. **23**: GB1010. doi:10.1029/2008gb003221

Leynaert, A. 1993. La production de silice biogénique dans l'océan: Se la mer de Weddell à l'océan Antarctique. Thèse de doctorat. Paris 6.

Leynaert, A., P. Tréguer, D. M. Nelson, and Y. Del Amo. 1996. ^{32}Si as a tracer of biogenic silica production: Methodological improvements. In: Integrated Marine System Analysis. Brussel: Vrije Universiteit.

Lindemann, C., Ø. Fiksen, K. H. Andersen, and D. L. Aksnes. 2016. Scaling laws in phytoplankton nutrient uptake affinity. Front. Mar. Sci. **3**: 26. doi:10.3389/fmars.2016.00026

Llopis Monferrer, N., and others. 2021. Role of small Rhizaria and diatoms in the pelagic silica production of the Southern Ocean. Limnol. Oceanogr. **66**: 2187–2202. doi:10.1002/lno.11743

Llopis-Monferrer, N., D. Boltovskoy, P. Tréguer, M. M. Sandin, F. Not, and A. Leynaert. 2020. Estimating biogenic silica production of Rhizaria in the Global Ocean. Global Biogeochem. Cycl. **34**: e2019GB006286. doi:10.1029/2019gb006286

Mansour, J. S., A. Norlin, N. L. Monferrer, S. L'Helguen, and F. Not. 2021. Carbon and nitrogen content to biovolume relationships for marine protist of the Rhizaria lineage (Radiolaria and Phaeodaria). Limnol. Oceanogr. **66**: 1703–1717. doi:10.1002/lno.11714

Marron, A. O., S. Ratcliffe, G. L. Wheeler, R. E. Goldstein, N. King, F. Not, C. de Vargas, and D. J. Richter. 2016. The evolution of silicon transport in eukaryotes. Mol. Biol. Evol. **33**: 3226–3248. doi:10.1093/molbev/msw209

Menden-Deuer, S., and E. J. Lessard. 2000. Carbon to volume relationships for dinoflagellates, diatoms, and other protist

plankton. Limnol. Oceanogr. **45**: 569–579. doi:10.4319/lo.2000.45.3.0569

Michaels, A. F., D. A. Caron, N. R. Swanberg, F. A. Howse, and C. M. Michaels. 1995. Planktonic sarcodines (Acantharia, Radiolaria, Foraminifera) in surface waters near Bermuda: Abundance, biomass and vertical flux. J. Plankton Res. **17**: 131–163. doi:10.1093/plankt/17.1.131

Miklasz, K. A., and M. W. Denny. 2010. Diatom sinkings speeds: Improved predictions and insight from a modified Stokes' single law. Limnol. Oceanogr. **55**: 2513–2525. doi:10.4319/lo.2010.55.6.2513

Mortlock, R. A., and P. N. Froelich. 1989. A simple method for the rapid determination of biogenic opal in pelagic marine sediments. Deep Sea Res. Part A Oceanogr. Res. Pap. **36**: 1415–1426. doi:10.1016/0198-0149(89)90092-7

Nakamura, Y., I. Imai, A. Yamaguchi, A. Tuji, F. Not, and N. Suzuki. 2015. Molecular phylogeny of the widely distributed marine protists, Phaeodaria (Rhizaria, Cercozoa). Protist **166**: 363–373. doi:10.1016/j.protis.2015.05.004

Nakamura, Y., and N. Suzuki. 2015. Phaeodaria: Diverse marine Cercozoans of world-wide distribution, p. 223–249. *In* Marine protists. Springer Japan. doi:10.1007/978-4-431-55130-0_9

Nakamura, Y., R. Somiya, N. Suzuki, M. Hidaka-Umetsu, A. Yamaguchi, and D. J. Lindsay. 2017. Optics-based surveys of large unicellular zooplankton: A case study on radiolarians and phaeodarians. Plankton Benthos Res. **12**: 95–103. doi:10.3800/pbr.12.95

Nakamura, Y., I. Iwata, R. S. Hori, N. Uchiyama, A. Tuji, M. J. Fujita, D. Honda, and H. Ohfuji. 2018. Elemental composition and ultrafine structure of the skeleton in shell-bearing protists—A case study of phaeodarians and radiolarians. J. Struct. Biol. **204**: 45–51. doi:10.1016/j.jsb.2018.06.008

Pondaven, P., M. Gallinari, S. Chollet, E. Bucciarelli, G. Sarthou, S. Schultes, and F. Jean. 2007. Grazing-induced changes in cell wall silicification in a marine diatom. Protist **158**: 21–28. doi:10.1016/j.protis.2006.09.002

R Core Team. 2020. R: A language and environment for statistical computing. R Foundation for Statistical Computing.

Redfield, A. C. 1934. On the proportions of organic derivatives in sea water and their relation to the composition of plankton. Liverpool Univ. Press.

Sierra, R., M. V. Matz, G. Aglyamova, L. Pillet, J. Decelle, F. Not, C. de Vargas, and J. Pawlowski. 2013. Deep relationships of Rhizaria revealed by phylogenomics: A farewell to Haeckel's Radiolaria. Mol. Phylogenet. Evol. **67**: 53–59. doi:10.1016/j.ympev.2012.12.011

Siever, R., S. H. Schneider, and P. J. Boston. 1991. Silica in the oceans: Biological-geochemical interplay. *In* Scientists on Gaia. MIT Press, Cambridge, MA.

Sterner, R. W., and J. J. Elser. 2017. Ecological stoichiometry. Princeton Univ. Press.

Strelkov, A., and V. Reshetnyak. 1959. Novaya zhiznennaya forma u radiolyariy. Zool. Zhur. **38**: 355–361.

Stukel, M. R., T. Biard, J. Krause, and M. D. Ohman. 2018. Large Phaeodaria in the twilight zone: Their role in the carbon cycle. Limnol. Oceanogr. **63**: 2579–2594. doi:10.1002/lno.10961

Sugiyama, K., and O. R. Anderson. 1997. Experimental and observational studies of radiolarian physiological ecology, 6. Effects of silicate-supplemented seawater on the longevity and weight gain of spongiose radiolarians *Spongaster tetras* and *Dictyocoryne truncatum*. Mar. Micropaleontol. **29**: 159–172. doi:10.1016/S0377-8398(96)00011-4

Suzuki, N., and F. Not. 2015. Biology and ecology of radiolaria, p. 179–222. *In* Marine protists. Springer Japan.

Takahashi, K., and S. Honjo. 1983. Radiolarian skeletons: Size, weight, sinking speed, and residence time in tropical pelagic oceans. Deep Sea Res. Part A Oceanogr. Res. Pap. **30**: 543–568. doi:10.1016/0198-0149(83)90088-2

Tréguer, P., L. Lindner, A. J. van Bennekom, A. Leynaert, M. Panouse, and G. Jacques. 1991. Production of biogenic silica in the Weddell-Scotia Seas measured with ^{32}Si. Limnol. Oceanogr. **36**: 1217–1227. doi:10.4319/lo.1991.36.6.1217

Tréguer, P. J., and others. 2021. Reviews and syntheses: The biogeochemical cycle of silicon in the modern ocean. Biogeosciences **18**: 1269–1289. doi:10.5194/bg-18-1269-2021

Yuasa, T., and O. Takahashi. 2016. Light and electron microscopic observations of the reproductive swarmer cells of nassellarian and spumellarian polycystines (Radiolaria). Eur. J. Protistol. **54**: 19–32. doi:10.1016/j.ejop.2016.02.007

Acknowledgments

The authors thank the captain, crew and science team of the R. V. *Roger Revelle* during the CCE-LTER P2107 cruise. The authors particularly thank M. Décima, S. Matthews and G. Cawley for their help in sampling. The authors are grateful to the CCE-LTER (National Science Foundation grants OCE-1637632 and OCE-1614359) program and its lead PI M. Ohman without whom this research would not have been possible. This work was supported by the "Agence Nationale de la Recherche" projects RhiCycle (ANR-19-CE01-0006) and ISblue (ANR-17-EURE-0015).

Conflict of Interest

None declared.

Submitted 22 August 2022
Revised 16 November 2022
Accepted 25 November 2022

Associate editor: Jana Hinners

Elemental content allometries and silicon uptake rates of planktonic Rhizaria: insights into their ecology and role in biogeochemical cycles – Supporting Information

Manon Laget[1], Natalia Llopis-Monferrer[2], Jean-François Maguer[2], Aude Leynaert[2], Tristan Biard[1]

[1] LOG, Laboratoire d'Océanologie et de Géosciences, Univ. Littoral Côte d'Opale, Univ. Lille, CNRS, IRD, UMR 8187, Wimereux, France.
[2] Univ. Brest, CNRS, IRD, Ifremer, LEMAR, F-29280, Plouzané, France

1 Sampling details

Table 1: Sampling nets used during the CCE-LTER P2107 cruise

Date	Latitude	Longitude	Gear	Depth range (m)
14/07/2021	33.8064	-120.4189	MOCNESS	400-600
17/07/2021	36.2005	-123.036	DeepNet	700-1000
17/07/2021	36.5122	-122.273	DeepNet	300-500
18/07/2021	36.5196	-122.2968	MOCNESS	400-600
21/07/2021	35.7467	-121.6759	RingNet	0-400
23/07/2021	36.1346	-122.102	BongoNet	0-500
24/07/2021	36.1927	-122.4567	RingNet	0-500
27/07/2021	36.0881	-122.3225	MOCNESS	300-600
28/07/2021	36.316	-122.7499	MOCNESS	350-450

2 Image analysis

Table 2: Assigned shapes for rhizarian taxa

Group	Taxon	Shape
Radiolaria	Spumellaria	cylinder
	Phlebarachnium sp.	prolate ellipsoid
	Oroscena sp.	prolate ellipsoid
	Cytocladus sp.	sphere
	solitary Collodaria	sphere
Phaeodaria	Aulacanthidae	sphere
	Aulosphaeridae	sphere
	Castanellidae	sphere
	Tuscaroridae	prolate ellipsoid
	Coelodendridae	sphere
	Medusettidae	sphere or sum of spheres for colonies
	Protocystis sp. (type 1)	prolate ellipsoid
	Protocystis sp. (type 2)	sphere

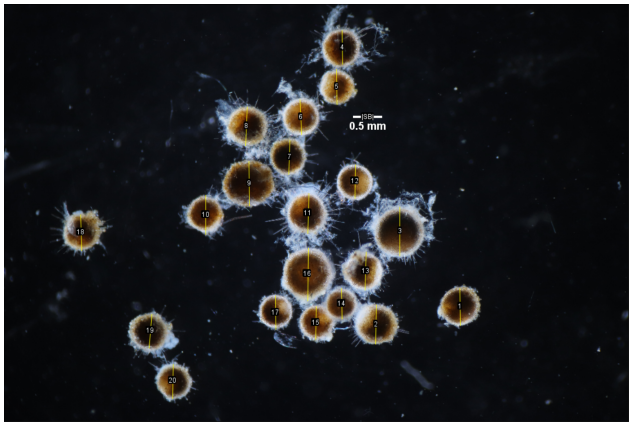

(a) Sample of Castanellidae

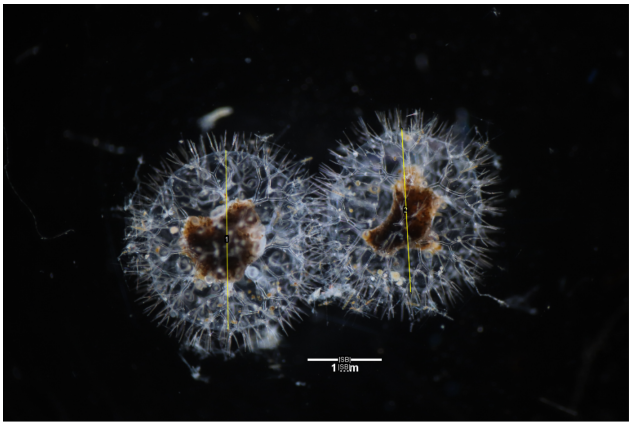

(b) Sample of Coelodendridae

Figure 1: Light microscopy photographs of Rhizaria specimens to describe the methodology for cell measurements

For non spherical objects, the Equivalent Spherical Diameter (ESD) was computed from the volume V as:

$$ESD = \left(\frac{3}{4} \times \frac{V}{\pi}\right)^{\frac{1}{3}} \times 2 \tag{1}$$

3 Silica data from literature

Table 3: Biogenic silica content data available from literature

Type	Mean cell vol. (mm)	nmol Si cell^{-1}	μg Si cell^{-1}	Area*	Reference
Aulacanthidae CCE	0.1	12.46	0.83	CCE	Biard et al., 2018
Aulacanthidae CCE	0.13	13.85	0.93	CCE	Biard et al., 2018

Aulacanthidae CCE	0.08	7.48	0.5	CCE	Biard et al., 2018
Aulacanthidae CCE	0.07	7.21	0.48	CCE	Biard et al., 2018
Aulacanthidae CCE	0.14	52.5	3.52	CCE	Biard et al., 2018
Aulacanthidae CCE	0.1	11.67	0.78	CCE	Biard et al., 2018
Aulacanthidae CCE	0.07	6.01	0.4	CCE	Biard et al., 2018
Aulacanthidae CCE	0.15	12.06	0.81	CCE	Biard et al., 2018
Aulacanthidae CCE	0.14	11.19	0.75	CCE	Biard et al., 2018
Aulacanthidae CCE	0.11	7.76	0.52	CCE	Biard et al., 2018
Aulacanthidae CCE	0.11	24.76	1.66	CCE	Biard et al., 2018
Aulacanthidae CCE	0.21	22.62	1.52	CCE	Biard et al., 2018
Theoperidae	0.2	8.61	0.58	CCE	Biard et al., 2018
Theoperidae	0.14	5.47	0.37	CCE	Biard et al., 2018
Castanellidae	0.17	242.62	16.26	CCE	Biard et al., 2018
Castanellidae	0.16	225.83	15.13	CCE	Biard et al., 2018
Castanellidae	0.17	219.21	14.69	CCE	Biard et al., 2018
Castanellidae	0.16	248.29	16.64	CCE	Biard et al., 2018
Castanellidae	0.14	234.75	15.73	CCE	Biard et al., 2018
Aulosphaeridae	7.27	235.87	15.8	CCE	Biard et al., 2018
Aulosphaeridae	7.36	278.41	18.65	CCE	Biard et al., 2018
Aulosphaeridae	5.39	158.75	10.64	CCE	Biard et al., 2018
Aulosphaeridae	6.25	215.92	14.47	CCE	Biard et al., 2018
Aulosphaeridae	5.59	160.8	10.77	CCE	Biard et al., 2018
Aulosphaeridae	10.74	127.6	8.55	CCE	Biard et al., 2018
Aulosphaeridae	6.7	247.16	16.56	CCE	Biard et al., 2018
Aulosphaeridae	8.2	286.7	19.21	CCE	Biard et al., 2018
Aulosphaeridae	2.25	93.74	6.28	CCE	Biard et al., 2018
Aulosphaeridae	5.62	220.31	14.76	CCE	Biard et al., 2018
Aulosphaeridae	7.83	98.34	6.59	CCE	Biard et al., 2018
Aulosphaeridae	1.45	55.1	3.69	CCE	Biard et al., 2018
Medusettidae	26.45	648.02	43.42	CCE	Biard et al., 2018
Aulosphaeridae	5.54	107.27	7.19	CCE	Biard et al., 2018
Coelodendridae	5.6	265.72	17.8	CCE	Biard et al., 2018
Aulosphaeridae	5.7	109.09	7.31	CCE	Biard et al., 2018
Aulosphaeridae	4.86	109.09	7.31	CCE	Biard et al., 2018
Aulosphaeridae	1.53	75.69	5.07	CCE	Biard et al., 2018
Aulosphaeridae	1.56	67.61	4.53	CCE	Biard et al., 2018
Aulosphaeridae	4.02	77.85	5.22	CCE	Biard et al., 2018
Aulosphaeridae	5.4	115.49	7.74	CCE	Biard et al., 2018
Aulosphaeridae	9.67	326.86	21.9	CCE	Biard et al., 2018
Aulosphaeridae	6.72	265.72	17.8	CCE	Biard et al., 2018
Aulosphaeridae	1.41	81.18	5.44	CCE	Biard et al., 2018
Aulosphaeridae	1.61	130.5	8.74	CCE	Biard et al., 2018
Aulosphaeridae	2.42	91.59	6.14	CCE	Biard et al., 2018
Aulosphaeridae	0.94	68.57	4.59	CCE	Biard et al., 2018
Aulosphaeridae	5.45	257.99	17.29	CCE	Biard et al., 2018
Aulacanthidae CCE	0.24	39.95	2.68	CCE	Biard et al., 2018
Aulacanthidae CCE	0.3	65.52	4.39	CCE	Biard et al., 2018
Aulacanthidae CCE	0.11	52.53	3.52	CCE	Biard et al., 2018
Aulacanthidae CCE	0.13	41.05	2.75	CCE	Biard et al., 2018
Aulacanthidae CCE	0.13	41.75	2.8	CCE	Biard et al., 2018
Aulacanthidae CCE	0.14	27.73	1.86	CCE	Biard et al., 2018
Aulacanthidae CCE	0.09	52.37	3.51	CCE	Biard et al., 2018
Coelodendridae	0.21	39.95	2.68	CCE	Biard et al., 2018
Coelodendridae	0.15	39.13	2.62	CCE	Biard et al., 2018
Coelodendridae	0.15	31.6	2.12	CCE	Biard et al., 2018
Coelodendridae	0.15	31.48	2.11	CCE	Biard et al., 2018
Coelodendridae	0.18	54.64	3.66	CCE	Biard et al., 2018
Castanellidae	0.05	190.2	12.74	CCE	Biard et al., 2018
Aulosphaeridae	1.74	354.3	23.74	CCE	Biard et al., 2018
Castanellidae	0.1	243.3	16.3	CCE	Biard et al., 2018

Castanellidae	0.07	175.6	11.77	CCE	Biard et al., 2018
Aulosphaeridae	0.72	137.3	9.2	CCE	Biard et al., 2018
Castanellidae	0.05	173.6	11.63	CCE	Biard et al., 2018
Collodaria	0.0042	1.65	0.11	Med	Llopis-Monferrer et al., 2020
Collodaria	0.0023	1.04	0.07	Med	Llopis-Monferrer et al., 2020
Collodaria	0.0006	0.37	0.02	Med	Llopis-Monferrer et al., 2020
Collodaria	0.0024	0.81	0.05	Med	Llopis-Monferrer et al., 2020
Collodaria	0.0012	0.96	0.06	Med	Llopis-Monferrer et al., 2020
Collodaria	0.0013	2.63	0.18	Med	Llopis-Monferrer et al., 2020
Nassellaria	0.0003	2.15	0.14	Med	Llopis-Monferrer et al., 2020
Nassellaria	0.0003	3.23	0.22	Med	Llopis-Monferrer et al., 2020
Nassellaria	0.0003	1.08	0.07	Med	Llopis-Monferrer et al., 2020
Spumellaria	0.0031	12.64	0.85	Med	Llopis-Monferrer et al., 2020
Spumellaria	0.0037	9.27	0.62	Med	Llopis-Monferrer et al., 2020
Spumellaria	0.0006	0.81	0.05	Med	Llopis-Monferrer et al., 2020
Spumellaria	0.0004	1.62	0.11	Med	Llopis-Monferrer et al., 2020
Aulacanthidae Med.	0.2730	42.97	2.88	Med	Llopis-Monferrer et al., 2020
Aulacanthidae Med.	0.3830	23.33	1.56	Med	Llopis-Monferrer et al., 2020
Aulacanthidae Med.	0.1453	24.62	1.65	Med	Llopis-Monferrer et al., 2020
Aulacanthidae Med.	0.4943	35.51	2.38	Med	Llopis-Monferrer et al., 2020
Aulacanthidae Med.	0.3103	16.62	1.11	Med	Llopis-Monferrer et al., 2020
Aulacanthidae Med.	0.5738	29.93	2.01	Med	Llopis-Monferrer et al., 2020
Aulacanthidae Med.	0.4928	16.59	1.11	Med	Llopis-Monferrer et al., 2020
Aulacanthidae Med.	0.4604	16.83	1.13	Med	Llopis-Monferrer et al., 2020
Aulacanthidae Med.	0.1724	59.63	3.99	Med	Llopis-Monferrer et al., 2020
Aulacanthidae Med.	0.1724	16.33	1.09	Med	Llopis-Monferrer et al., 2020
Aulacanthidae Med.	0.1724	22.29	1.49	Med	Llopis-Monferrer et al., 2020
Aulacanthidae Med.	0.1724	9.39	0.63	Med	Llopis-Monferrer et al., 2020
Aulacanthidae Med.	0.4100	25.22	1.69	Med	Llopis-Monferrer et al., 2020
Aulacanthidae Med.	0.3115	24.64	1.65	Med	Llopis-Monferrer et al., 2020
Aulacanthidae Med.	0.3115	21.68	1.45	Med	Llopis-Monferrer et al., 2020
Aulacanthidae Med.	0.3115	31.58	2.12	Med	Llopis-Monferrer et al., 2020
Aulacanthidae Med.	0.3115	26.45	1.77	Med	Llopis-Monferrer et al., 2020
Protocystis Med.	0.0072	9.04	0.61	Med	Llopis-Monferrer et al., 2020
Protocystis Med.	0.0007	1.59	0.11	Med	Llopis-Monferrer et al., 2020
Protocystis Med.	0.0002	2.03	0.14	Med	Llopis-Monferrer et al., 2020
Protocystis Med.	0.0005	1.06	0.07	Med	Llopis-Monferrer et al., 2020
Protocystis Med.	0.0005	1.73	0.12	Med	Llopis-Monferrer et al., 2020

* CCE stands for California Current Ecosystem and Med for Mediterranean Sea.

4 Excess densities and sinking speeds

The excess density (μg mm^{-3}) of an organism is given by:

$$\sigma_{cell} = \rho_{cell} - \rho_{sw} \tag{2}$$

with ρ_{cell} the density of the cell and ρ_{sw} the density of seawater. For these calculations, we assumed that density of seawater was 1027.5 kg m^{-3} in the Mediterranean Sea (salinity = 37, temperature = 15°C) and 1025.2 kg m^{-3} in the California Current (salinity = 34, temperature = 15°C).

According to Baines et al. (2010) and Stukel et al. (2018), we computed the cell densities as follows:

$$\rho_{cell} = \frac{M_{cell}}{V_{cell}} \tag{3}$$

V_{cell} the cellular volume (mm^3) was expressed as:

$$V_{cell} = V_{skel} + V_{om} + V_w \tag{4}$$

V_{cell} was directly measured on photos. V_{skel} and V_{om} were deduced from the elemental mass and the assumed excess densities of 2.15 g ml^{-1} for biogenic silica and 1.05 g ml^{-1} for organic matter, i.e.:

$$V_{skel} = \frac{Q_{bSi}}{2.15 \times 10^{-3}} \tag{5}$$

$$V_{om} = \frac{Q_C + Q_N}{1.05 \times 10^{-3}} \tag{6}$$

with Q_{bSi}, Q_C and Q_N the bSi, C and N contents in μg cell^{-1}, respectively.

M_{cell} the cellular mass (μg) was expressed as:

$$M_{cell} = M_{skel} + M_{om} + M_w \tag{7}$$

with $M_{skel} = Q_{bSi}$, $M_{om} = Q_C + Q_N$ and $M_w = \rho_{sw} \times V_w$.

The theoretical sinking speeds U_{th} (in m s^{-1}) were computed from Stokes' Law (Stokes, 1851) as:

$$U_{th} = \frac{1}{18} \frac{g(\rho_{cell} - \rho_{sw}) ESD^2}{\mu_{sw}} \tag{8}$$

with $g = 9.81$ m s^2 the gravitational acceleration and $\mu_{sw} = 0.001$ Pa s the assumed dynamic viscosity of the fluid.

5 Elemental content-to-volume relationships: residual analysis

5.1 Carbon

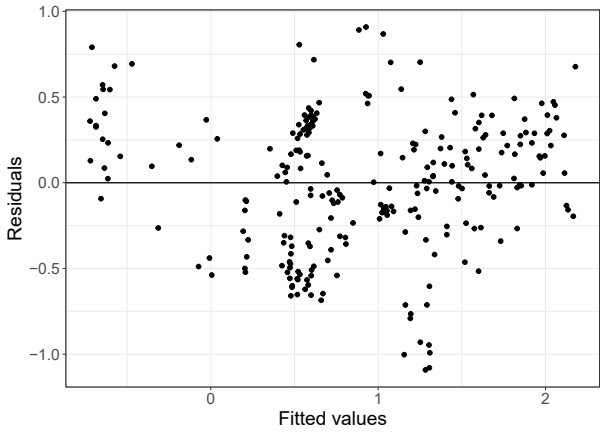

(a) Residuals as a function of fitted values

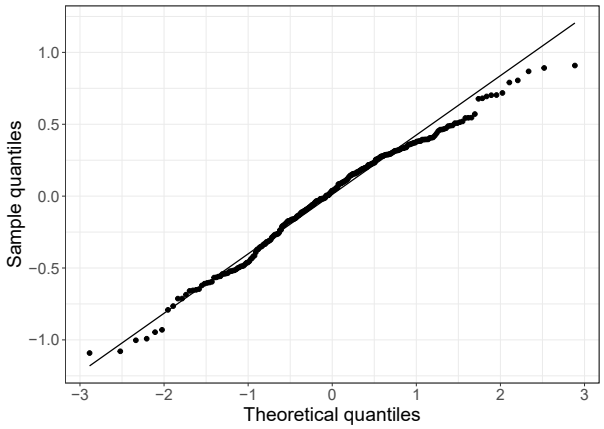

(b) Quantile-quantile plot

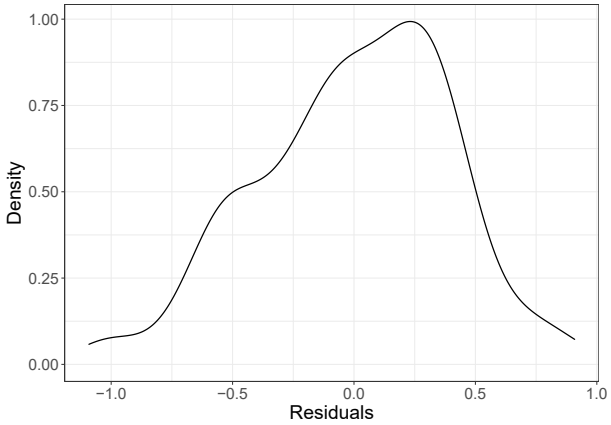

(c) Density plot of the residuals

Figure 2: Residual analysis for the model 1 least-squares regression of $\log_{10}$–transformed Q_C (μg C cell^{-1}) to V (mm^3) for Rhizaria specimens including solitary cells and colonies.

5.2 Nitrogen

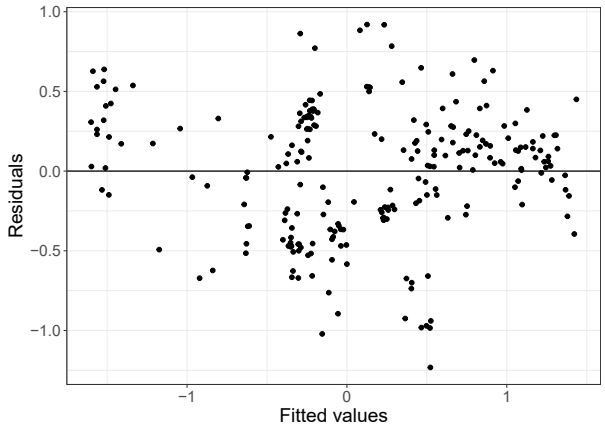

(a) Residuals as a function of fitted values

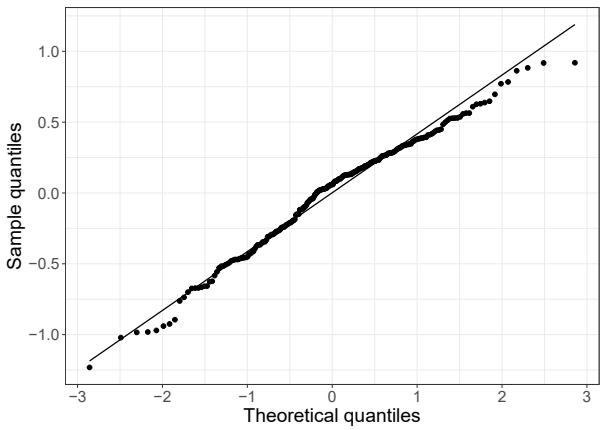

(b) Quantile-quantile plot

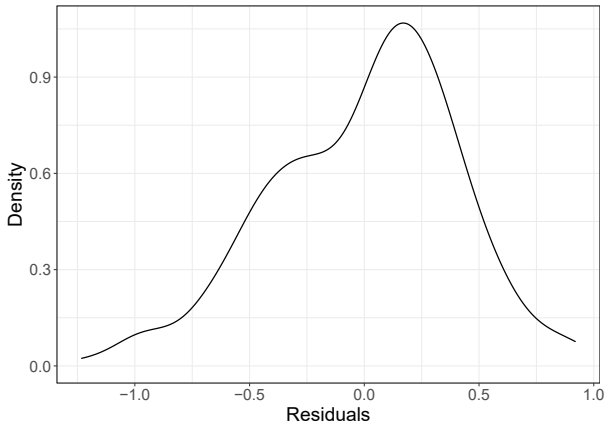

(c) Density plot of the residuals

Figure 3: Residual analysis for the model 1 least-squares regression of $\log_{10}$–transformed Q_N (μg N cell^{-1}) to V for Rhizaria specimens including solitary cells and colonies.

6 Comparison of models for Phaeodaria and Radiolaria

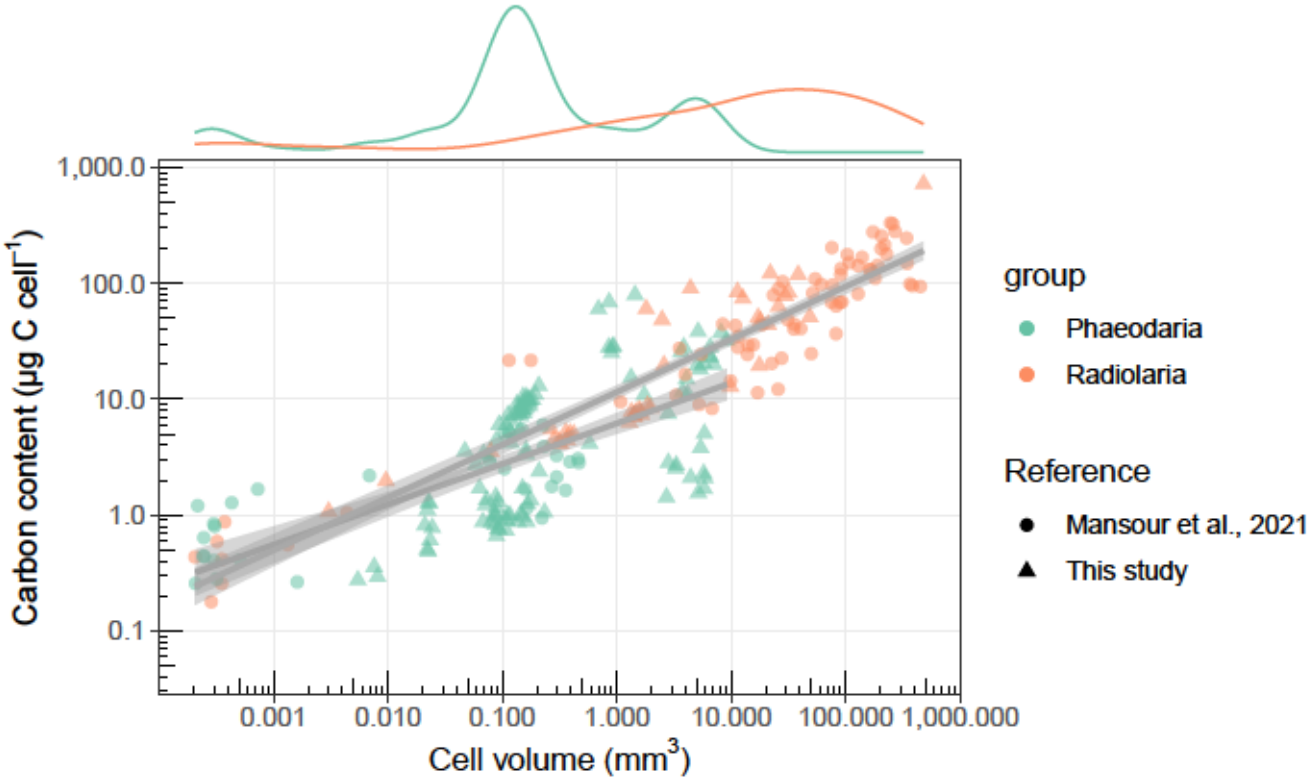

Figure 4: Model 1 least-squares regression of $\log_{10}$–transformed Q_C (μg C cell^{-1}) to V (mm^3) for Radiolaria and Phaeodaria considered separately. Grey area represents the 95% confidence level intervals for predictions. Above density plots show the repartition of data per group. Data are compiled from Mansour et al. (2021) and this study.

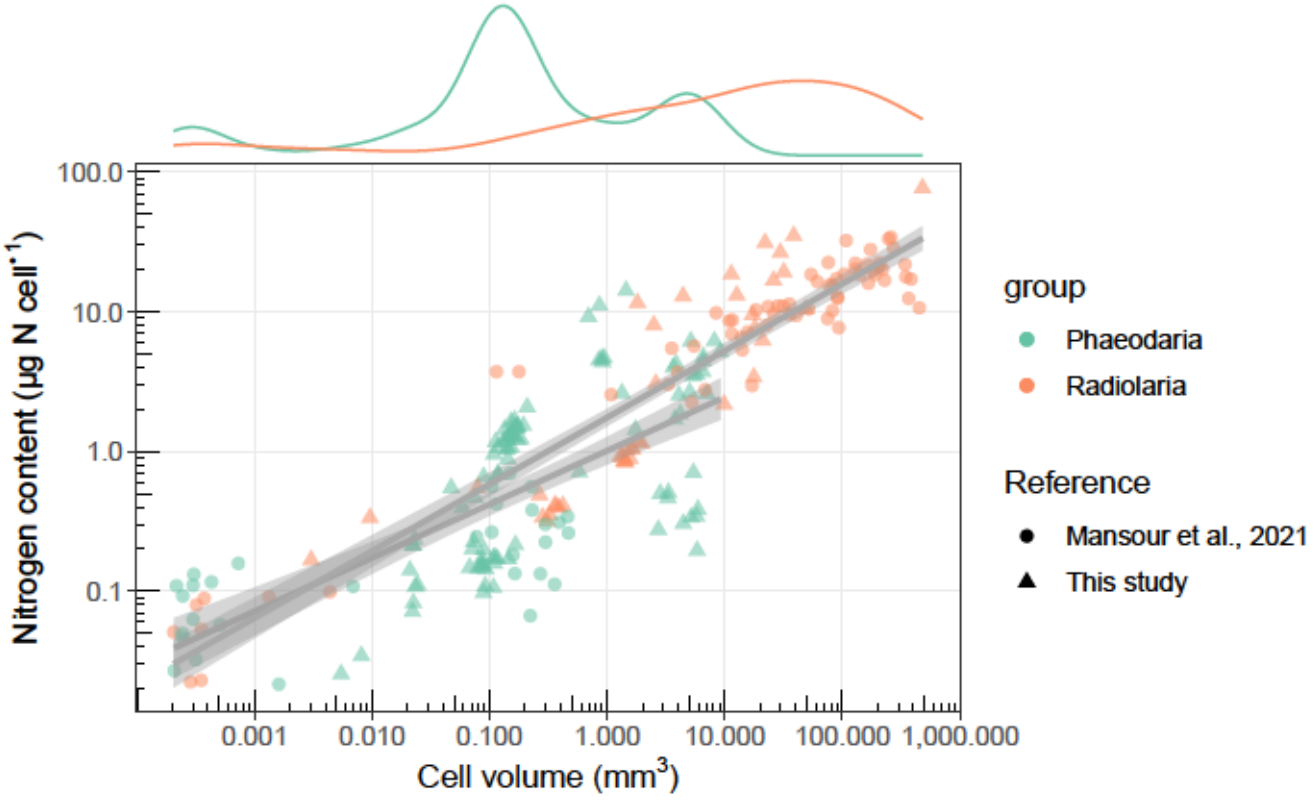

Figure 5: Model 1 least-squares regression of $\log_{10}$–transformed Q_N (μg N cell^{-1}) to V (mm^3) for Radiolaria and Phaeodaria considered separately. Grey area represents the 95% confidence level intervals for predictions. Above density plots show the repartition of data per group. Data are compiled from Mansour et al. (2021) and this study.

Table 4: Equations from models 1 ordinary least-squares regression of $\log_{10}$-transformed Q_C or Q_N (μg C cell^{-1} or μg N cell^{-1}) to V (mm^3) for Radiolaria and Phaeodaria considered separately. Data are compiled from Mansour et al. (2021) and this study.

Group	Equation	R^2
Radiolaria C	$\log_{10} Q_C = [1.06 \pm 0.03] + [0.45 \pm 0.02] \times \log_{10} V$	0.866
Phaeodaria C	$\log_{10} Q_C = [0.79 \pm 0.05] + [0.35 \pm 0.03] \times \log_{10} V$	0.435
Radiolaria N	$\log_{10} Q_N = [0.24 \pm 0.03] + [0.48 \pm 0.02] \times \log_{10} V$	0.869
Phaeodaria N	$\log_{10} Q_N = [0.01 \pm 0.05] + [0.38 \pm 0.04] \times \log_{10} V$	0.482

7 Molar C:N ratios

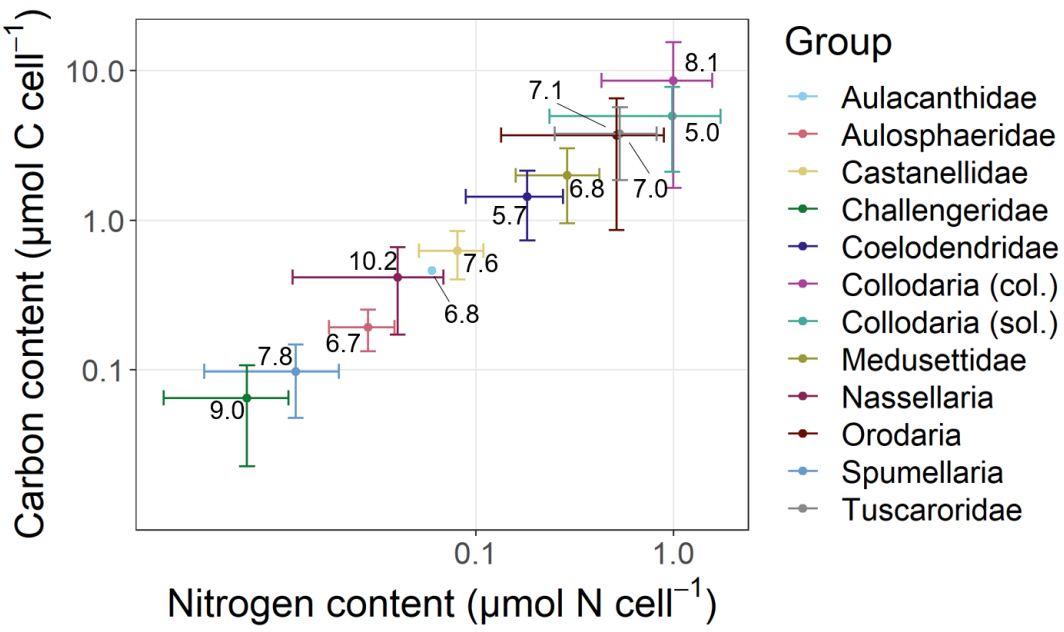

Figure 6: Mean carbon content (μmol C cell^{-1}) as a function of mean nitrogen content (μmol N cell^{-1}) for various Rhizaria taxa. Values are for each group the molar ratio of the mean carbon content to the mean nitrogen content. Error bars show mean ± standard error. Data are compiled from Mansour et al. (2021) and this study.

8 Biogenic silica content and molar Si:C ratio

8.1 Biogenic silica content to volume allometry

The previous allometry was given by (Llopis-Monferrer et al., 2020):

$$\log_{10}(Q_{bSi}) = -4.05 + 0.52 \times \log_{10}(V) \tag{9}$$

with Q_{bSi} in μg Si cell^{-1} and V in μm^3.

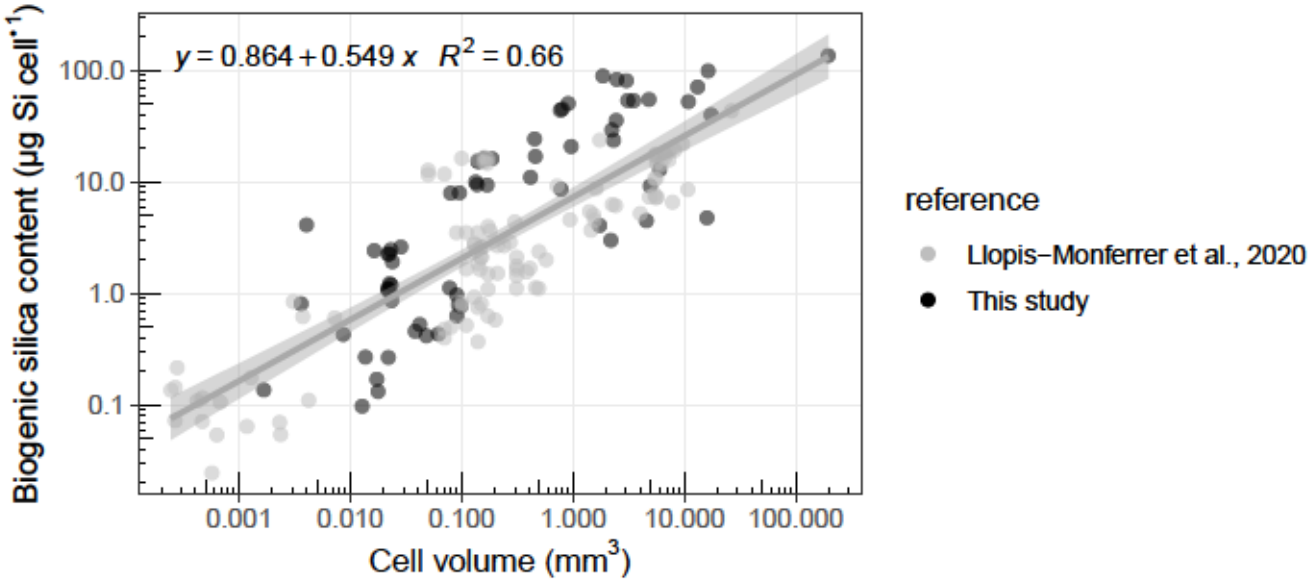

Figure 7: New model 1 least-squares regression of $\log_{10}$–transformed silica content (μg Si cell^{-1}) to cell volume (μm^3) for siliceous Rhizaria. Data are compiled from Llopis-Monferrer et al. (2020) and this study.

8.2 Molar Si:C ratio

Table 5: Summary of carbon and biogenic silica contents. Si:C ratio are calculated as the ratio of the median silica content to the median carbon content. Data are compiled from Biard et al. (2018), Llopis-Monferrer et al. (2020), Mansour et al. (2021) and this study.

Group	Taxon	Area*	n_C	Median nmol C cell^{-1}	Range nmol C cell^{-1}	n_{bSi}	Median nmol Si cell^{-1}	Range nmol Si cell^{-1}	Si:C
Phaeodaria	Aulacanthidae	CCE	24	84	54–3114	32	26	6–1479	0.31
	Aulacanthidae	Med	27	208	78–500	17	24	9–59	0.12
	Aulosphaeridae	CCE	10	182	118–316	34	129	44–595	0.71
	Castanellidae	CCE	35	640	112–1086	19	225	118–248	0.35
	Coelodendridae	CCE	13	970	73–2337	10	60	31–819	0.06
	Medusettidae	CCE	3	1504	1277–3179	1	648	648–648	0.43
	Challegenridae (*Protocystis* sp.)	CCE	11	50	22–106	13	17	6–39	0.34
	Tuscaroridae	CCE	7	2367	2093–6596	7	656	164–1331	0.28
Radiolaria	Nassellaria (*Phlebarachnium* sp.)	CCE	19	589	343–730	10	4	1–7	0.01
	Orodaria (*Oroscena* sp.)	CCE	5	4029	292–7507	2	654	71–1238	0.16
	Spumellaria	CCE	2	126	89–164	1	61	61–61	0.48

* CCE stands for California Current Ecosystem and Med for Mediterranean Sea.

9 Silicon uptake rates ρ_{Si}

Table 6: Summary data of biogenic Si contents (Q_{bSi}), Si uptake rates (ρ_{Si}) and Si specific uptake rates (V_{Si}) from this study.

Group	Taxon	n	ESD[1,2] (μm)	Q_{bSi} [1] (nmol Si cell^{-1})	ρ_{Si} [1] (nmol Si cell^{-1} d^{-1})	V_{Si} [1] (d^{-1})
Phaeodaria	Aulacanthidae	4	832 ± 558	142.52 ± 259.73	0.46 ± 0.70	0.0077 ± 0.0079
	Aulosphaeridae	6	1948 ± 736	193.37 ± 204.47	0.62 ± 0.54	0.0056 ± 0.0074
	Castanellidae	3	655 ± 43	232.95 ± 7.33	0.17 ± 0.11	0.0007 ± 0.0005
	Challegenridae (*Protocystis* sp.)	1	353	36.95	0.07	0.0020
Radiolaria	Collodaria	1	7209	2024.30	4.31	0.0021
	Nassellaria (*Phlebarachnium* sp.)	10	346 ± 99	4.35 ± 2.35	0.31 ± 0.25	0.0647 ± 0.0350
	Orodaria (*Oroscena* sp.)	1	1678	1238.69	0.81	0.0007

[1] Values are expressed as mean ± standard error. [2] Equivalent Spherical Diameter.

Table 7: Daily averaged silicic acid concentration measured from sample collected with Niskin bottles.

Date (GMT)	Silicic acid conc. (μmol L^{-1})	Minimum depth (m)	Maximum depth (m)
18/07/2021	14.96400	5.495	80.958
24/07/2021	20.88050	3.738	522.860
25/07/2021	20.13625	4.832	519.776
29/07/2021	21.78250	5.015	518.891
30/07/2021	17.63312	4.737	519.135
03/08/2021	12.05937	4.721	522.432
04/08/2021	11.84625	5.311	519.642
06/08/2021	12.29625	5.488	520.188
10/08/2021	17.55813	5.392	204.520

Table 8: Detailed data and metadata of biogenic Si contents (Q_{bSi}), Si uptake rates (ρ_{Si}) and Si specific uptake rates (V_{Si}) from this study.

Latitude	Longitude	Gear	Date	Depth range (m)	Taxon	n^1	ESD^2 (μm)	Volume (μm^3)	ρ_{Si} (nmol Si cell^{-1} d^{-1})	Q_{bSi} (nmol Si cell^{-1})	V_{Si} (d^{-1})
		DeepNet	18/07/2021	1000 - 50	Aulosphaeridae	2	1606	2187105107	0.92	0.045	0.0205
36.3241	-122.7686	RingNet	24/07/2021	500 - 0	Aulacanthidae	14	561	98737338	0.22	0.012	0.0192
36.3241	-122.7686	RingNet	24/07/2021	500 - 0	Aulacanthidae	1	1671	2443025342	1.50	0.532	0.0028
36.3241	-122.7686	RingNet	24/07/2021	500 - 0	Castanellidae	4	643	141379762	0.30	0.228	0.0013
36.3241	-122.7686	RingNet	24/07/2021	500 - 0	Aulosphaeridae	4	1121	780518746	0.58	0.128	0.0045
36.3241	-122.7686	RingNet	24/07/2021	500 - 0	Aulosphaeridae	1	3215	17399004222	1.54	0.596	0.0026
36.1676	-122.4665	Mocness	25/07/2021	600 - 400	*Protocystis* sp.	5	353	23088581	0.07	0.037	0.0020
36.6044	-123.4352	Bongo	29/07/2021	300 - 0	Aulacanthidae	15	554	93152137	0.07	0.012	0.0063
36.6044	-123.4352	Bongo	29/07/2021	300 - 0	Aulacanthidae	18	546	90229089	0.04	0.015	0.0025
36.6044	-123.4352	Bongo	29/07/2021	300 - 0	Aulosphaeridae	3	1490	1737189540	0.23	0.061	0.0038
36.6044	-123.4352	Bongo	29/07/2021	300 - 0	Castanellidae	5	620	139534319	0.12	0.230	0.0005
36.6044	-123.4352	Bongo	29/07/2021	300 - 0	Orodaria	1	1678	2474195264	0.81	1.239	0.0007
36.705	-123.0394	RingNet	30/07/2021	300 - 0	Aulosphaeridae	13	2014	4939335975	0.10	0.137	0.0007
36.705	-123.0394	RingNet	30/07/2021	300 - 0	Castanellidae	9	704	187127543	0.10	0.241	0.0004
34.7136	-130.5414	RingNet	03/08/2021	50 - 0	Nassellaria	25	144	1669750	0.24	0.002	0.1185
34.7136	-130.5414	RingNet	03/08/2021	50 - 0	Nassellaria	25	293	13655738	0.25	0.004	0.0613
34.7136	-130.5414	RingNet	03/08/2021	300 - 0	Nassellaria	25	428	42002596	0.46	0.008	0.0580
34.7136	-130.5414	RingNet	03/08/2021	300 - 0	Nassellaria	25	412	38251196	0.51	0.007	0.0744
34.6385	-130.5178	RingNet	04/08/2021	50 - 0	Nassellaria	25	282	12748444	0.07	0.001	0.0505
34.6385	-130.5178	RingNet	04/08/2021	50 - 0	Nassellaria	30	316	17736047	0.06	0.002	0.0297
34.6385	-130.5178	RingNet	04/08/2021	300 - 0	Nassellaria	25	446	48186747	0.63	0.006	0.1004
34.6385	-130.5178	RingNet	04/08/2021	300 - 0	Nassellaria	25	484	61693415	0.70	0.006	0.1075
34.5029	-130.4235	RingNet	06/08/2021	300 - 0	Nassellaria	20	344	21931830	0.10	0.004	0.0256
34.5029	-130.4235	RingNet	06/08/2021	300 - 0	Nassellaria	20	317	17296937	0.05	0.003	0.0212
35.2885	-121.3928	SalpNet	10/08/2021	350 - 0	Collodaria	1	7209	1.96166E+11	4.31	2.024	0.0021
35.2885	-121.3928	SalpNet	10/08/2021	350 - 0	Aulosphaeridae	6	2248	6015315528	0.32	0.193	0.0017

[1] Number of specimens per sample. [2] Equivalent Spherical Diameter.

References

Baines, S. B., B. S. Twining, M. A. Brzezinski, D. M. Nelson, and N. S. Fisher (2010). Causes and biogeochemical implications of regional differences in silicification of marine diatoms. In: *Global Biogeochemical Cycles* 24.4 (cit. on p. 4).

Biard, T., J. W. Krause, M. R. Stukel, and M. D. Ohman (2018). The Significance of Giant Phaeodarians (Rhizaria) to Biogenic Silica Export in the California Current Ecosystem. In: *Global Biogeochemical Cycles* 32.6, pp. 987–1004. DOI: 10.1029/2018gb005877 (cit. on pp. 2–4, 12).

Llopis-Monferrer, N., D. Boltovskoy, P. Tréguer, M. M. Sandin, F. Not, and A. Leynaert (2020). Estimating Biogenic Silica Production of Rhizaria in the Global Ocean. In: *Global Biogeochemical Cycles* 34.3. DOI: 10.1029/2019gb006286 (cit. on pp. 4, 10–12).

Mansour, J. S., A. Norlin, N. Llopis Monferrer, S. l'Helguen, and F. Not (2021). Carbon and nitrogen content to biovolume relationships for marine protist of the Rhizaria lineage (Radiolaria and Phaeodaria). In: *Limnology and Oceanography* 66.5, pp. 1703–1717 (cit. on pp. 8–10, 12).

Stokes, G. G. (1851). On the effect of the internal friction of fluids on the motion of pendulums. Vol. 9. Trans. Cambridge Philos. Soc. (cit. on p. 5).

Stukel, M. R., T. Biard, J. Krause, and M. D. Ohman (2018). Large Phaeodaria in the twilight zone: Their role in the carbon cycle. In: *Limnology and Oceanography* 63.6, pp. 2579–2594 (cit. on p. 4).